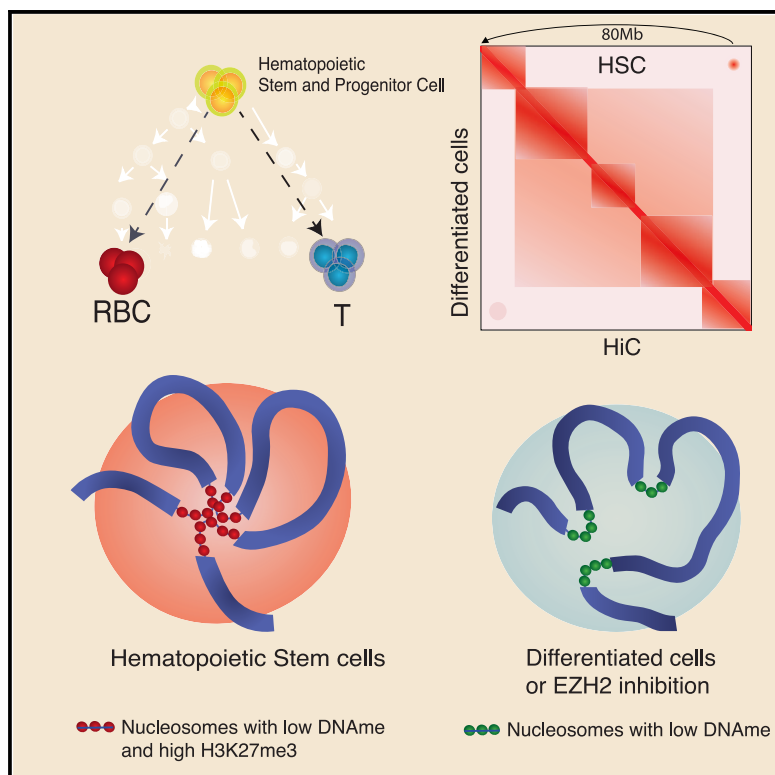


Large DNA Methylation Nadirs Anchor Chromatin Loops Maintaining Hematopoietic Stem Cell Identity

Graphical Abstract



Authors

Xiaotian Zhang, Mira Jeong,
Xingfan Huang, ..., Jianzhong Su,
Erez Lieberman Aiden,
Margaret A. Goodell

Correspondence

zxtzhangqian@gmail.com (X.Z.),
erez@erez.com (E.L.A.),
goodell@bcm.edu (M.A.G.)

In Brief

Zhang et al. discovered that very large DNA methylation nadirs (grand canyons) form megabase-scale and inter-chromosomal 3D genomic interactions in primary stem and progenitor cells. H3K27me3 is strongly enriched in grand canyons and is important for organizing the grand canyon interactions associated with their stem cell state.

Highlights

- Long DNA methylation canyons (grand canyons) form megabase-scale 3D genomic interactions
- Grand canyon 3D interactions are specific to primary stem and progenitor cells
- Grand canyon 3D interactions do not require CTCF and cohesion
- High H3K27me3 levels in grand canyons are required for their interactions



Large DNA Methylation Nadirs Anchor Chromatin Loops Maintaining Hematopoietic Stem Cell Identity

Xiaotian Zhang,^{1,4,17,*} Mira Jeong,^{1,2,17} Xingfan Huang,^{3,7,16,17} Xue Qing Wang,⁴ Xinyu Wang,⁵ Wanding Zhou,⁴ Muhammad S. Shamim,^{3,6,7} Haley Gore,⁴ Pamela Himadewi,⁴ Yushuai Liu,⁴ Ivan D. Bochkov,^{3,8} Jaime Reyes,^{1,2,8} Madison Doty,⁹ Yung-Hsin Huang,^{1,2,10} Haiyoung Jung,^{1,2,11} Emily Heikamp,^{1,2,12} Aviva Presser Aiden,^{3,10,12} Wei Li,^{13,14} Jianzhong Su,⁵ Erez Lieberman Aiden,^{3,7,8,15,*} and Margaret A. Goodell^{1,2,8,12,14,18,*}

¹Stem Cells and Regenerative Medicine Center, Baylor College of Medicine, Houston, TX, USA

²Center for Cell and Gene Therapy, Baylor College of Medicine, Houston, TX, USA

³The Center for Genome Architecture, Baylor College of Medicine, Houston, TX, USA

⁴Center for Epigenetics, Van Andel Institute, Grand Rapids, MI, USA

⁵Institute of Biomedical Big Data, Wenzhou Medical University, Wenzhou, China

⁶Medical Student Training Program, Baylor College of Medicine, Houston, TX, USA

⁷Center for Theoretical Biological Physics & Department of Computer Science, Rice University, Houston, TX, USA

⁸Department of Molecular and Human Genetics, Baylor College of Medicine, Houston, TX, USA

⁹Molecular Genetic Technology Program, School of Health Professions, The University of Texas MD Anderson Cancer Center, Houston, TX, USA

¹⁰Developmental Biology Program, Baylor College of Medicine, Houston, TX, USA

¹¹Immunotherapy Convergence Research Center, Korea Research Institute of Bioscience and Biotechnology, Yuseong-gu, Daejeon, Korea, USA

¹²Department of Pediatrics, Baylor College of Medicine, Houston, TX, USA

¹³Department of Bioinformatics, Biological Chemistry, University of California, Irvine CA, USA

¹⁴Department of Molecular and Cellular Biology, Baylor College of Medicine, Houston, TX, USA

¹⁵Shanghai Institute for Advanced Immunochemical Studies, Shanghai Tech University, Shanghai, China

¹⁶Present address: University of Washington, Seattle, WA, USA

¹⁷These authors contributed equally

¹⁸Lead Contact

*Correspondence: zxtzhangqian@gmail.com (X.Z.), erez@erez.com (E.L.A.), goodell@bcm.edu (M.A.G.)

<https://doi.org/10.1016/j.molcel.2020.04.018>

SUMMARY

Higher-order chromatin structure and DNA methylation are implicated in multiple developmental processes, but their relationship to cell state is unknown. Here, we find that large (>7.3 kb) DNA methylation nadirs (termed “grand canyons”) can form long loops connecting anchor loci that may be dozens of megabases (Mb) apart, as well as inter-chromosomal links. The interacting loci cover a total of ~3.5 Mb of the human genome. The strongest interactions are associated with repressive marks made by the Polycomb complex and are diminished upon EZH2 inhibitor treatment. The data are suggestive of the formation of these loops by interactions between repressive elements in the loci, forming a genomic subcompartment, rather than by cohesion/CTCF-mediated extrusion. Interestingly, unlike previously characterized subcompartments, these interactions are present only in particular cell types, such as stem and progenitor cells. Our work reveals that H3K27me3-marked large DNA methylation grand canyons represent a set of very-long-range loops associated with cellular identity.

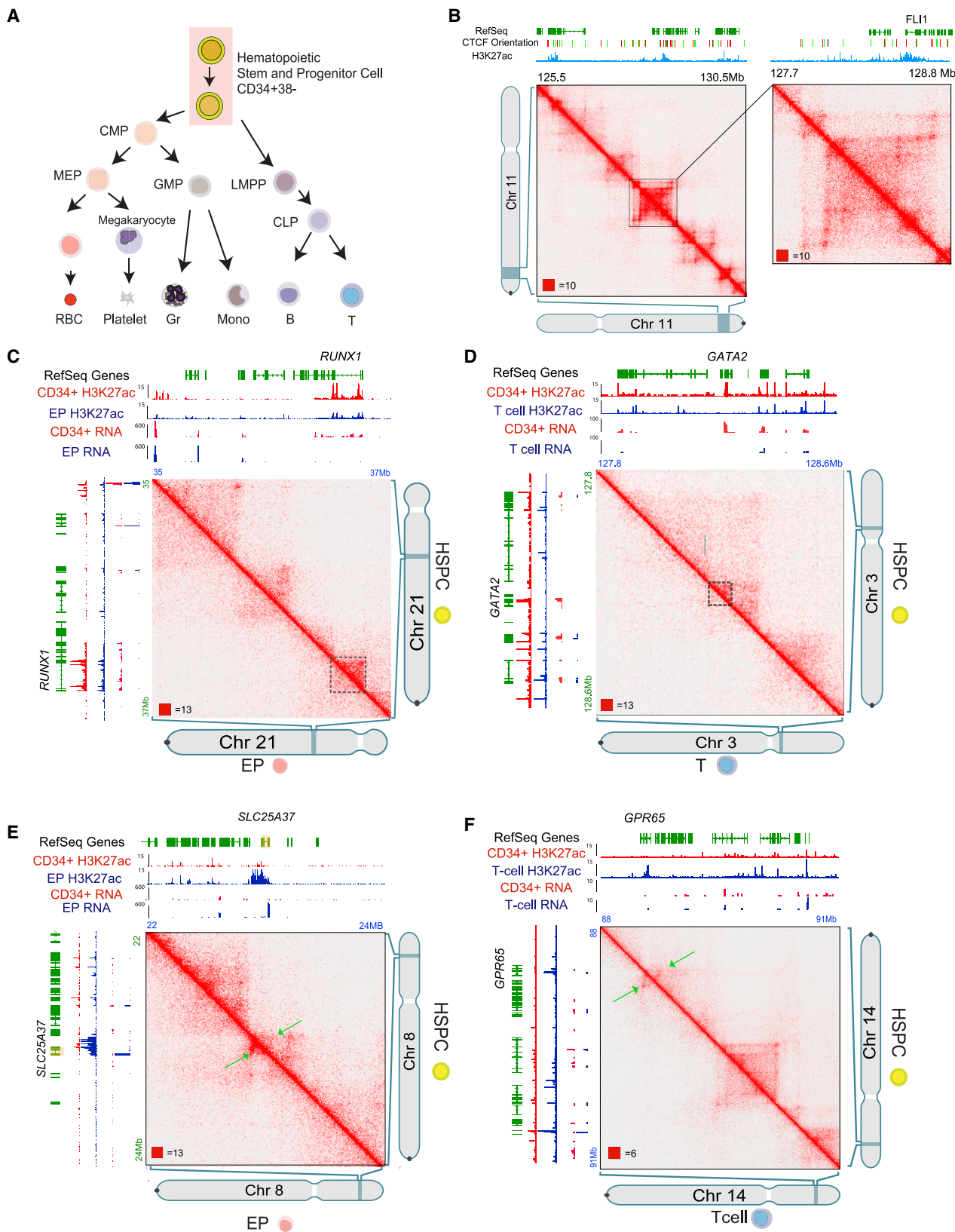
INTRODUCTION

In the human genome, cytosine residues located in CpG dinucleotides are often, but not always, methylated (5-methyl-C). CpG islands—genomic intervals, typically 300–3,000 bp in length, containing many CpG dinucleotides—are an important exception (Bird *et al.*, 1985). Frequently located near promoters, CpG islands are typically unmethylated when the nearby gene is active. Yet despite extensive study, the mechanisms that under-

lie the relationship between DNA methylation and gene transcription remain poorly understood.

One possibility is that the absence of DNA methylation leads to changes in three-dimensional (3D) chromatin architecture that influence transcription. In recent years, experiments combining DNA-DNA proximity ligation with high-throughput sequencing (Hi-C) have made it possible to generate high-resolution maps of chromatin architecture by measuring the frequency of contacts between all pairs of loci, genome-wide (Cullen *et al.*,





(legend on next page)

1993; Dixon et al., 2012, 2015; Lieberman-Aiden et al., 2009; Rao et al., 2014). These experiments have revealed two mechanisms of chromatin folding. The first is associated with the formation of a class of loops between sites bound by cohesin and CTCF, such that the CTCF motifs lie in the convergent orientation (i.e., they point toward one another) (Fudenberg et al., 2016; Sanborn et al., 2015). To explain this phenomenon, it has been hypothesized that cohesin initially forms small loops between nearby sites, which grow larger through a process of extrusion until an inward-pointing CTCF is encountered (Alipour and Marko, 2012; Fudenberg et al., 2016; Nasmyth, 2001; Nichols and Corces, 2015; Sanborn et al., 2015). The second mechanism is compartmentalization: the tendency of genomic intervals with similar histone modifications to co-segregate in three dimensions inside the nucleus (Lieberman-Aiden et al., 2009; Rao et al., 2014).

We were interested in exploring a potential relationship between DNA methylation and genome architecture, but the typical CpG island is too short to be reliably interrogated using Hi-C, preventing the exploration of these features. However, we recently identified exceptionally long genomic intervals (~3.5–25 kb) that exhibit low levels of cytosine methylation, dubbed “DNA methylation canyons” (Jeong et al., 2014) (also known as DNA methylation valleys; Xie et al., 2013). Canyons, which often contain multiple CpG islands, are strongly preserved across cell types and species. In any given cell, particular canyons are typically either repressed, and decorated with H3K27me3, or active, and decorated with H3K4me3 (Jeong et al., 2014).

Because of their unusual size, DNA methylation canyons are a natural system for exploring the influence of methylation on genome architecture. Moreover, the DNA methyltransferases regulating canyon size are highly expressed in hematopoietic stem and progenitor cells (HSPCs) and are important for their differentiation (Challen et al., 2011; Jeong et al., 2014). HSPCs and their downstream progeny are well characterized, offering primary cells in which 3D architecture can be explored within a differentiation hierarchy.

Performing *in situ* Hi-C experiments at 10 kb resolution, we observe the formation of hundreds of long-range loops between large, repressed canyons lying on the same chromosome, as well as evidence for links between canyons located on different chromosomes. Taken together, our data are consistent with the formation of a unique set of contacts in which large DNA methylation canyons from across the genome tend to co-segregate. We show that these features are present, albeit much weaker, after HSPC differentiation and in other differentiated cell types. Our findings indicate that DNA methylation works in tandem with histone modifications to influence the 3D architecture of the human genome.

RESULTS

Generation of High-Resolution Contact Maps in Hematopoietic Progenitors and Differentiated Cells

We first sought to generate a high-resolution contact map in primary human HSPCs. We purified HSPCs from human umbilical cord blood (UCB) as lineage-negative CD34+ CD38– cells (Figures 1A and S1A) and generated *in situ* Hi-C libraries (Rao et al., 2014) yielding ~1B read pairs representing 613M Hi-C contacts (Table S1) and processed the data using Juicer (Durand et al., 2016b). For comparisons with HSPCs, we also isolated differentiated T cells (CD3+) and erythroid progenitors (EPs; via directed differentiation and sorting for CD36+ CD71+ CD235a+) (Figures 1A and S1B–S1D). Our initial analysis showed compartments, contact domains, and loops, each connecting a pair of loop anchor points on the same chromosome as reported for other cells (Figures 1B and S1E).

Comparing HSPCs and differentiated progeny, we found that the position of contact domains was not altered significantly (Figures S1F and S1G). However, intra-contact domain interactions were distinct around lineage-specific genes. In HSPCs, intra-domain interactions are extensive in regions associated with key HSPC-associated genes and enhancers (Figures 1C and 1D), such as the ~1 Mb *RUNX1* locus (Figure 1C) and the *GATA2* locus. Thus, these maps will serve as a resource for HSPC 3D interactions (e.g., KLF12; Figure S2A).

In differentiated cells, we observed loops associated with cell-type-specific genes and H3K27ac-enhancer marks (Figures 1E and 1F). More intra-domain interactions were evident when cell type-specific genes were expressed. For instance, *SLC25A37*, a mitochondrial iron transporter, formed an a contact domain only in EPs (Figure 1E). Similarly, a contact domain at *GPR65*, which has a role in T cells (Choi et al., 1996), was absent in HSPCs (Figure 1F). Strong interactions around stem cell-specific genes such as *RUNX1* were decreased in differentiated cells (Figures 1C and 1D).

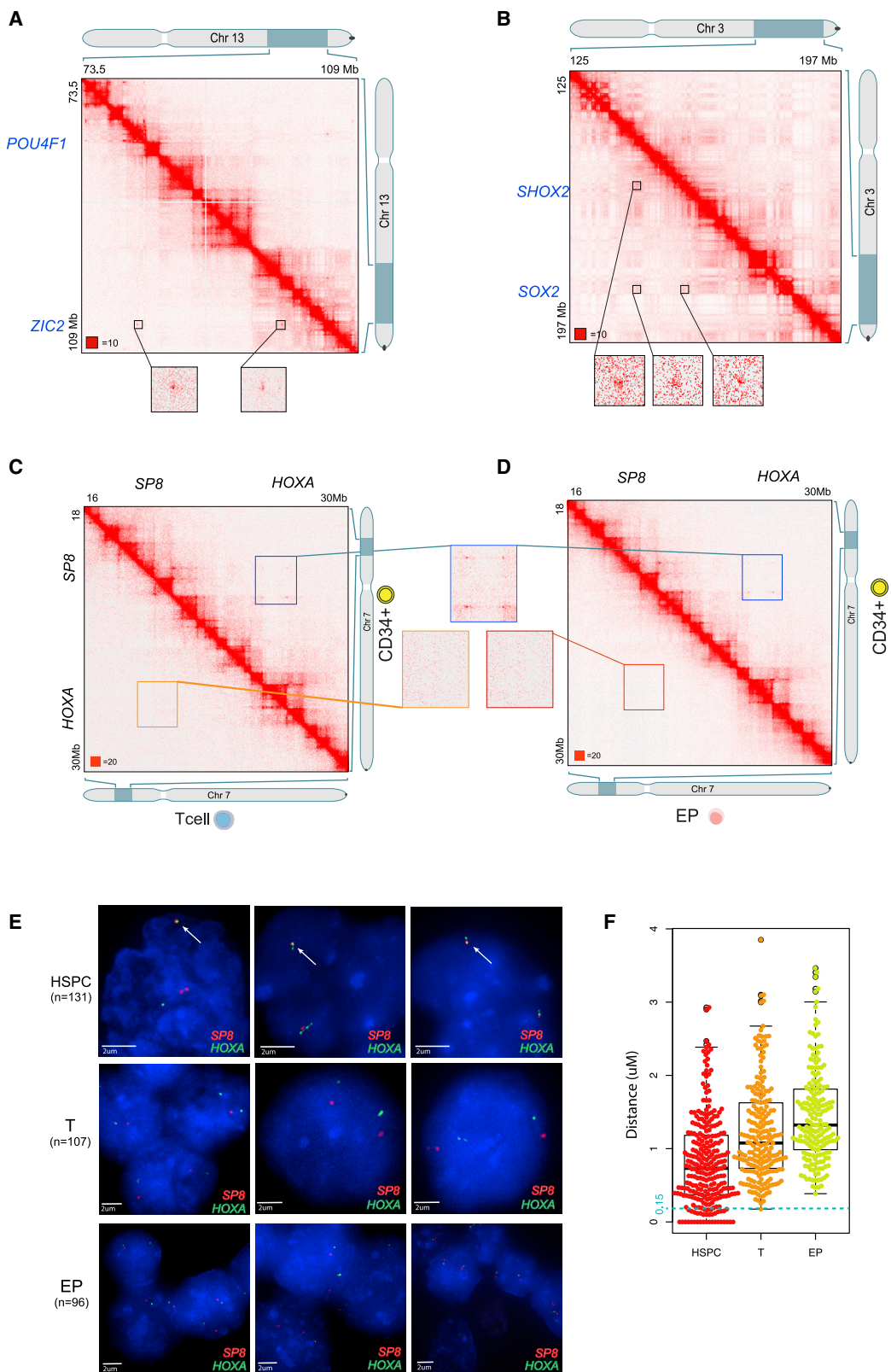
Discovery of Long Loops Specifically in HSPCs

Upon further scrutiny, we identified sites of very long distance interactions, well beyond the distance of ~2 Mb typically associated with cohesin-associated loops (Rao et al., 2014). For example, we observed interactions among *SHOX* (Chr3:158MB), *SOX2* (Chr3:181MB), and the *POU3F3* (Chr2:105.4M) loci, approximately 23 Mb apart, and among *ZIC2* (Chr13:100M), *POU4F1* (Chr13:79M), and *PDX1* (Chr13:28M), approximately 72 Mb apart (Figures 2A, 2B, S2B, and S2C). To quantify these, we manually annotated the maps on all chromosomes to identify 408 loops whose anchors were >2 Mb apart (Table S2).

To confirm the presence of these long loops at the single-cell level, we performed 3D fluorescence *in situ* hybridization (FISH)

Figure 1. Very-Long-Range Interactions in the 3D HSPC Genome

- (A) Diagram of the hematopoietic hierarchy. HSPC was selected for Hi-C profiling.
- (B) An example of contacts from chromosome 11 at 10 kb resolution (left) and blowout at 5 kb resolution (right).
- (C) Example of chromosome loops around the stem cell-associated gene *RUNX1*. HSPCs (upper) and T cells (lower).
- (D) Example of chromosome loops around the stem cell-associated gene *GATA2*. HSPCs (upper) and EPs (lower).
- (E) Example of chromosome loops around the EP associated gene *SLC25A37*. HSPCs (upper) and EPs (lower).
- (F) Example of chromosome loops around the T cell-associated gene *GPR65*. HSPCs (upper) and T cells (lower).



(legend on next page)

using fluorescently labeled probes. We validated interactions between the *HOXD* and *DLX1* loci, separated by 4 Mb, using FISH probes, compared with a control probe within a similar distance. We observed close localization of *HOXD* and *DLX1* but not the control region (Video S1). Furthermore, we observed that another loop anchor, *PAX3*, which is 50 Mb away from *HOXD*, also simultaneously colocalized with *HOXD* and *DLX1* (Video S2). Together, these data reveal the presence of exceptionally long loops in HSPCs, with numerous anchors on the order of 50 Mb apart (median 7.5 Mb), with the largest being 117 Mb (Table S2) (average 15.8 Mb, range 2–117 Mb).

Loops or contact domains of this extraordinary size have rarely been reported except on the inactive X chromosome (Rao et al., 2014; Darrow et al., 2016). Therefore, we asked whether these were a general feature of primary hematopoietic cells. HSPC long loops were not apparent in T cells and EPs. To confirm their absence, we performed 3D FISH across all three cell types using two color probes that spanned the *HOXA* anchor and the *SP8* anchor, which are ~7 Mb apart (Figures 2C and 2D). Quantification of the average distance between signals showed the loci were closest in HSPCs (Figure 2E). We detected *HOXA*-*SP8* co-localization (signals \leq 0.15 μ m apart) in 20% of the HSPC nuclei but only 1% of T cells and 0% of EP. We observed similar results from *TWIST1*-*HOXA*, *DLX1*-*HOXD*, and *PAX3*-*DLX1*-*HOXD* loci (Figure S3A; Video S3). These data corroborate the Hi-C analysis indicating that the *SP8*-*HOXA* loci and *DLX1*-*HOXD* loci are in closer physical proximity in HSPCs compared with their differentiated progeny.

HSPC Long Loops Are Not Consistent with the Loop Extrusion Model

In order to investigate how long loops are formed and how they relate to loops mediated by CTCF extrusion, we examined their properties systematically. First, we used our standard loop-calling algorithm, HiCCUPS (Durand et al., 2016b; Rao et al., 2014), and identified 2,683 loops in HSPCs (Table S2; Figures 3A and 3B). Many of these loops overlapped with those reported in other cell types: 2,014 of these 2,683 loops overlapped the 9,448 loops reported in GM12878 cells, and 1,832 overlapped 8,040 loops reported in IMR90 cells. As in previous studies, the anchors were usually bound by CTCF (by chromatin immunoprecipitation sequencing [ChIP-seq], 74%, 4.1-fold enriched versus random controls of similar length), with the motifs in convergent orientation (for 2,534 of the 2,744 loop anchors with a unique CTCF

motif [92%], the motif points inward; $p = 6.07 \times 10^{-506}$). These observations confirmed the accuracy of our maps and the presence of typical features.

Interestingly, the CTCF-binding profile of the loop anchors identified using HiCCUPS depended on the size of the loop (i.e., linear distance). Whereas HSPC loops shorter than 1 Mb were bound by CTCF in 77.0% of cases (4.5-fold enrichment), loops longer than 3 Mb were bound by CTCF only 46.7% of the time (2.9-fold enrichment) (Figure 3E; Figures S3B and S3C). Similarly, longer loops were less likely to obey the convergent rule. For loops < 1 Mb, 95% of CTCF motifs at loop anchors pointed inward compared with only 57.9% for loops > 3 Mb (Figure 3F).

Most of the 408 manually annotated long loops (458 anchors) were not identified by our algorithms, so we manually examined and annotated their CTCF profiles. Anchors at long loops exhibited minimal enrichment for CTCF (1.04-fold; Figures 3C and 3D), and even when CTCF was bound, they did not obey the convergent rule (130 of 290 CTCF motifs [44.8%] pointed inward) (Figures 3C, 3D, and 3F) and were significantly longer than canonical cohesion extrusion loops (Figure 3G).

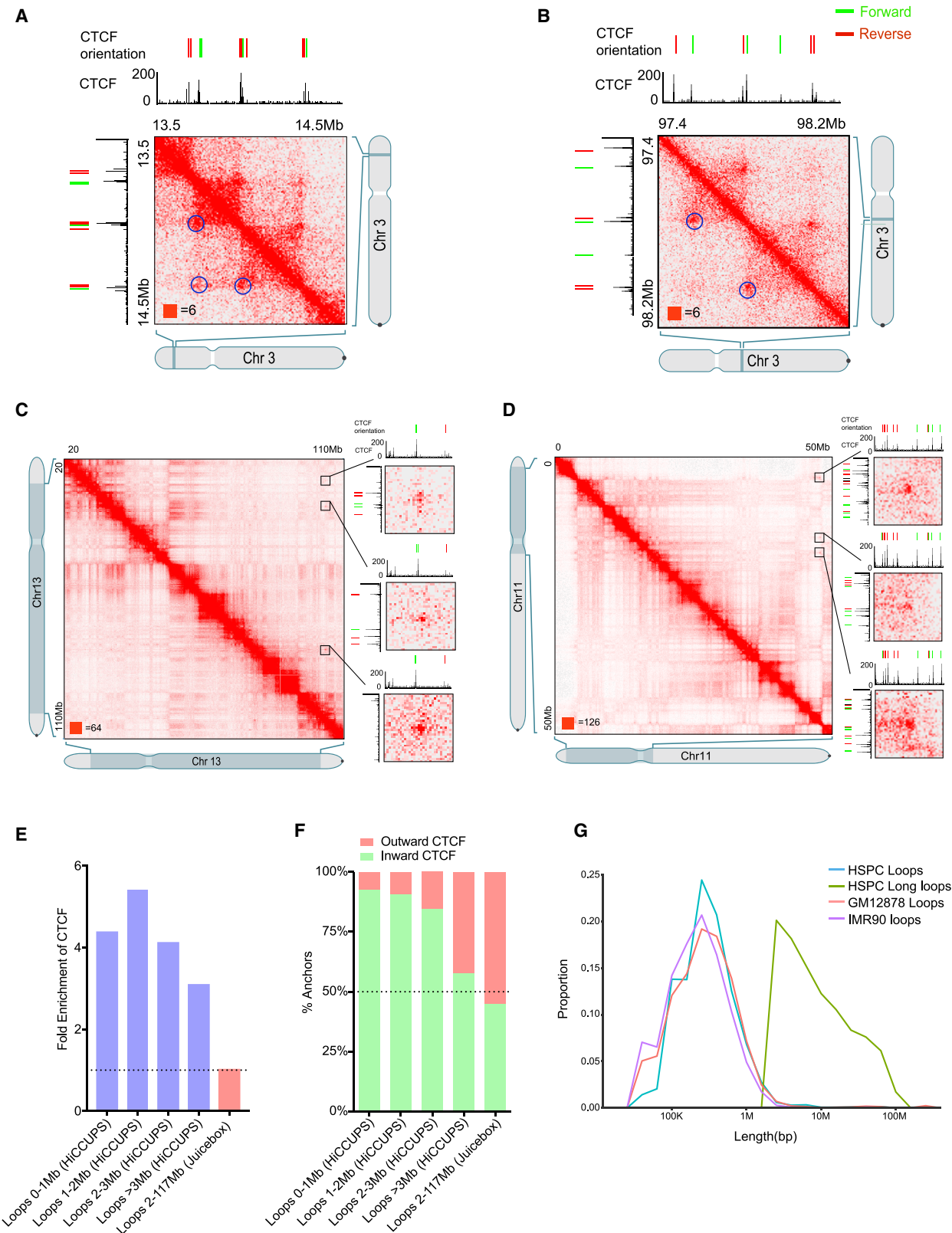
Importantly, we also tested if CTCF degradation affected grand canyon interactions. We performed aggregate peak analysis (APA) on data from mouse embryonic stem cells in which CTCF had been acutely degraded (Nora et al., 2017), finding that depletion of CTCF did not change the long-loop interactions (Figure S3E). Together, these findings suggest that long loops form in HSPCs by a mechanism independent of CTCF and cohesion.

DNA Methylation Canyons Lie at the Anchor of Long Loops

Next, we examined whether other features correlated with these long loops. By aligning DNA methylation profiles with the Hi-C data, we observed that anchors often corresponded to regions of very low DNA methylation (Table S3) and thus analyzed the relationship in detail. The anchor position of long loops had lower average DNA methylation levels than standard loop anchors (Figure S3D) and often overlapped with DNA methylation canyons (Figures 4A–4C). To quantify this, we compared the position of loop anchors with the 282 canyons longer than 7.3 kb (dubbed “grand canyons”), reasoning that shorter canyons might not reliably influence our HSPC contact map given the limitations of Hi-C resolution. Strikingly, we found that the rate of overlap with grand canyons depended strongly on the size of the loop.

Figure 2. Long Loops in HSPC and the Validation of Long-Range Interactions by 3D FISH

- (A) Example of intra multiple long-range interaction on chromosome 13. The matrices are shown at 100 kb resolution and blowout of *POU4F1* and *ZIC2* region at 5 kb resolution.
- (B) Example of intra multiple long-range interaction on chromosome 3. The matrices are shown at 100 kb resolution and blowout of *SHOX2* and *SOX2* region at 5 kb resolution.
- (C) Hi-C contact maps at *HOXA* cluster. HSPC-specific contact between *SP8* and the *HOXA* cluster is highlighted with green square. HSPCs (upper) and T cells (lower).
- (D) Hi-C contact maps at *HOXA* cluster. HSPC-specific contact between *SP8* and the *HOXA* cluster is highlighted with green square. HSPCs (upper) and EPs (lower).
- (E) Left panel: dual color DNA FISH with probes targeting *SP8* and repressive *HOXA* locus in HSPCs, T cells, and EP cells. Representative 3D DNA FISH images. *SP8* (red), *HOXA* (green), and DAPI (blue). Right panel: the distance between *SP8* and *HOXA* measured by FISH in HSPCs and T cells. p value is calculated using two-sample t test ($p = 2.08e-11$, HSC versus T; $p = 1.56e-22$, HSC versus EP).



(legend on next page)

Of the anchors of HSPC loops < 1 Mb, 1.8% overlapped a grand canyon (77 of 4,287, 4 \times enrichment). By contrast, 29.0% of anchors of HSPC loops > 3 Mb annotated by HiCCUPS overlapped a grand canyon, a 45-fold enrichment (18 of 62). Similarly, of the 458 manually annotated long loop anchors, 24% (110) overlapped a grand canyon (16.7-fold enrichment; Figure 4D).

Canyons are typically decorated with either active or repressive histone marks. We considered whether a particular group of canyons was associated with the long loops, performing ChIP-seq in HSPCs for histone marks indicative of repressive and active chromatin (H3K27me3 and H3K27ac, respectively). We found that nearly all grand canyons (85% [241 of 282]) exhibit broad H3K27me3, indicating a repressed state (Figure 4E). Further comparisons between shorter canyons and under-methylated regions (UMRs) showed that grand canyons have a distinctly high H3K27me3 signal, while being depleted of H3K27ac, distinguishing them from other CpG islands (Figure 4E). A small number instead exhibited broad H3K27ac indicating a more active state (18% [53 of 282]); these were much less likely to be involved in long loops relative repressed (H3K27me3) grand canyons (5 of 39 versus 100 of 227, respectively, a 3.4-fold depletion) (Table S3).

Because the loops forming between grand canyons were so long, we wondered whether they formed links to different chromosomes. To address this, we used APA to computationally superimpose Hi-C submatrices from the vicinity of multiple putative loops (Durand et al., 2016b; Rao et al., 2014), allowing contact frequencies to be visualized even when individual loops are not discernable. We thus examined pairs of grand canyons separated by varying linear distances, as well as pairs lying on different chromosomes. As controls, we examined anchors of HSPC short loops and anchors of previously published loops. We found that pairs of grand canyons tended to form loops regardless of their linear distance and to form links even when located on different chromosomes (Figure 4F). In contrast, the control anchors showed high APA scores only on the same chromosome and at distances < 2 Mb (Figure 4F). To determine the relevance of the Polycomb-mediated histone modification H3K27me3, we ran APA with UMRs enriched for H3K27me3. We found that these short repressive UMRs (srUMRs) did not show significant long-range interactions in comparison with repressive grand canyons. These data show that long loops are closely associated with DNA methylation grand canyons that primarily exhibit repressive histone marks and that repressive marks alone are insufficient to explain the interactions. Notably, the inter-chromosomal interactions are inconsistent with the loop extrusion model, which can facilitate only intra-molecular loops, not inter-molecular links.

EZH2 Inhibition Results in Loss of Grand Canyon Interactions

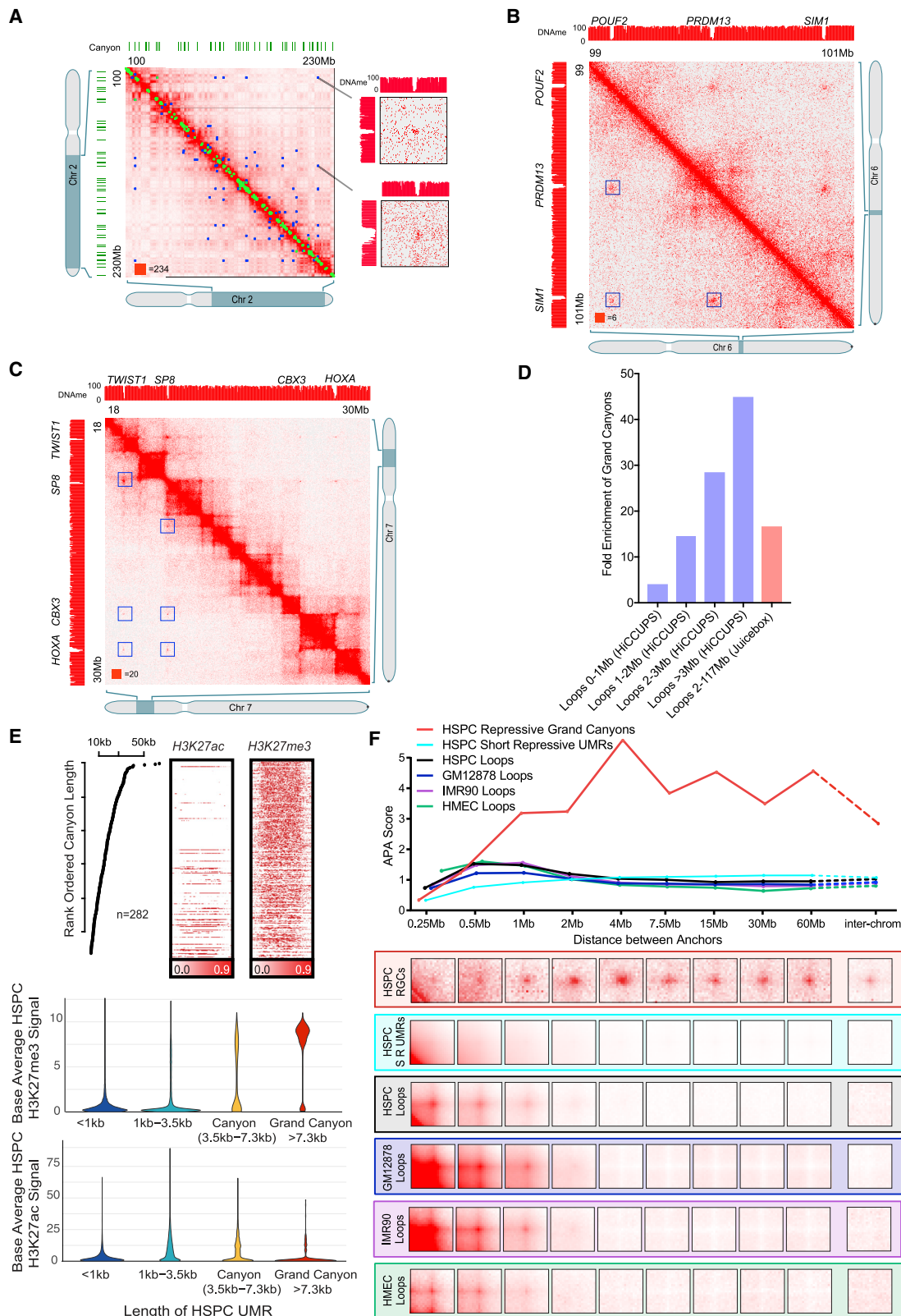
The observation that grand canyons with the highest levels of H3K27me3 enrichment are interacting suggests that this mark plays a key role in establishing these loops. To investigate this, we treated HSPCs with a small-molecule inhibitor of EZH2, EPZ6438 (Sneeringer et al., 2010), the main catalytic component of the PRC2 complex that generates the H3K27me3 mark. We reasoned that treatment with the inhibitor during modest *ex vivo* expansion of HSPCs would blunt the formation of H3K27me3 and potentially affect grand canyon interactions (Figure 5A). EZH2 inhibition revealed a global decrease of H3K27me3 at grand canyons (e.g., HOXC, PAX6, and WT1; Figure 5C), as well as at short canyons and UMRs ≤ 3.5 kb (Figure 5B). Furthermore, we observed weak activation of a few loci after EZH2 inhibitor treatment (Figure S4A). We then performed Hi-C on cells treated with vehicle or EPZ6438. Although *ex vivo* expansion diminished the grand canyon interactions to 73% of that observed in uncultured cells, EZH2 inhibition dramatically reduced the interactions to 22% of those in fresh HSPCs (Figure 5D). Meanwhile, the loss of H3K27me3 did not show any significant impact on CTCF-mediated loops (Figures 5D and 5E). These data suggest that the H3K27me3 deposited by EZH2 in grand canyon loci is essential for long-loop interaction. We also verified that the EZH2 inhibitor disrupted distribution of H3K27me3 in HSPCs. The H3K27me3 in DMSO treated cells formed patches overlapping with nucleus, especially on the periphery (Figure 5F). After EZH2 inhibitor treatment, these patches disappeared, and the H3K27me3 signal became very weak (Figure 5F). Next, we tested the distribution of PRC2 protein SUZ12 in DMSO and inhibitor-treated cells. We found that SUZ12 also formed foci and patches in the nucleus, but inhibitor treatment did not alter the foci and patches significantly (Figure S4B). This suggests that the loss of grand canyon interaction is due to the loss of H3K27me3 but not Polycomb complex binding per se. Overall, these data suggest that although the H3K27me3 marks generated by the Polycomb complex are important for long-range interactions, it is only those regions with the highest concentration, or the longest regions, that are able to participate in very-long-range contacts (Figure 5F; Figure S4C). We propose that a size of about 7.3 kb is the lower limit for repressed grand canyon loci to segregate together and expect a dependence on local H3K27me3 nucleosome concentration.

Long Loops Associated with Repressive Grand Canyons Are Limited to Primary Cells

Next, we considered whether HSPC long loops were present in other human cell types (Figure 6A). We used APA to re-analyze

Figure 3. Long Loops Are a Feature of 3D Genomic Interactions Independent of Cohesion Extrusion Loops in HSPC

- (A) Example of regular HiCCUPS loop with convergent CTCF motifs on chromosome 3 in the *WNT7A* region at 5 kb resolution.
- (B) Example of regular HiCCUPS loop with convergent CTCF motifs on chromosome 3 in the *GABRR3* region at 5 kb resolution.
- (C) Example of intra multiple long-range interaction on chromosome 13. The matrices are shown at 100 kb resolution and blowout of *CDX2*, *NBEA*, *POU4F1*, and *ZIC2* region at 10 and 5 kb resolution.
- (D) Example of intra multiple long-range interaction on chromosome 11. The matrices are shown at 100 kb resolution and blowout of *NUC160*, *NUC98*, *COPB1*, and *NUCB2* region at 10 and 5 kb resolution.
- (E) Fold enrichment of CTCF binding sites on loop anchors compared with random translational control regions (HiCCUPS loops, blue bars; long loops, red bar).
- (F) Inward and outward orientation of CTCF motifs on loop anchors.
- (G) Length distribution of HiCCUPS loops (blue line) versus long loops (green line) and loops identified in GM12878 (orange) and IMR90 (purple) cells.



(legend on next page)

a total of ~30 billion Hi-C read pairs from 19 human cell types in which loop-resolution Hi-C maps are available (Bonev et al., 2017; Darrow et al., 2016; Haarhuis et al., 2017; Rao et al., 2014, 2017; Sanborn et al., 2015). In every cell type examined, the aggregate signal was either absent (18 cell types) or nearly absent (GM12878 lymphoblastoid; diminished by 88%) (Figure 6B). In contrast, loops with convergent CTCF sites were preserved across cell types (except in HCT116 cells after cohesin degradation (Rao et al., 2017)).

To dissect why long loops are seen only in primary cells, we examined the level of H3K27me3 and DNA methylation in grand canyons, canyons, and UMRs < 3.5 kb. We found that HSPCs exhibit the highest H3K27me3 enrichment levels among human cell lines with available high-resolution Hi-C data (Figure 6D). In cancer cell lines (HCT116, HeLa, and K562), H3K27me3 was significantly lower in grand canyon regions. Other immortalized cell lines (GM12878, IMR90, and human primary epithelial mammary cells [HMECs]) as well as EPs also showed reduced H3K27me3. Although primary cells (normal human epidermal keratinocytes [NHEKs] and T cells) and IMR90 cells showed enrichment of H3K27me3 in grand canyons, the H3K27me3 level was still lower than in HSPCs (Figure 6D). Importantly, HSPCs also exhibited the lowest DNA methylation levels in grand canyons, while hypermethylation occurs in many cell lines (HMECs, IMR90, GM12878, K562, and HCT116). Regions flanking grand canyons were hypomethylated in K562 and GM12878 cell lines, consistent with their general global hypomethylation. DNA methylation in grand canyons increased mildly in EP and T cells (Figure 6E). Together, these data suggest that DNA methylation guides long-range grand canyon interactions, while Polycomb-associated H3K27me3 is critical to the formation of these loops (Figure 6E; Figure S5A).

We also used APA to analyze ten murine cell types in which loop-resolution Hi-C maps are available (>35 billion read pairs) (Bonev et al., 2017; Kieffer-Kwon et al., 2017). We observed strong conservation of long loops in mouse embryonic stem and neural progenitor cells (Bonev et al., 2017) (Figure 6C). All other more differentiated cell types had little or no discernable APA signal, except for activated (but not resting) B cells (Figures S6A–S6C). Together, this demonstrates a correlation between long loops and stem and progenitor cells. APA of the T cells and EPs from our study also confirmed that long loops were not evident in the progeny of human HSPCs (Figures S5B and S5C). Interestingly, in mouse somatic cells, we found that activated B cells also bear some grand canyon interactions. In these

cells, H3K27me3 in grand canyons is higher than resting B cells (Figure S5D), consistent with a Polycomb association.

A Stem Cell Grand Canyon Interaction Maintains HOXA Gene Expression

Finally, we sought to explore the functional significance of long loops by removing a grand canyon at a loop anchor. As most grand canyons are associated with promoters and exons, the functional impact of canyon deletion could be confounded by the effect gene loss. To obviate this concern, we identified a grand canyon lacking an obvious gene (“geneless” canyon [“GLS”]). The GLS is 17 kb long and lies 1.4 Mb upstream of the *HOXA1* gene (Figure 7A). In HSPCs, the GLS is coated with H3K27me3, lacks transcriptional activity, and interacts with multiple canyons (e.g., *TWIST* and *SP8*). GLS also interacts downstream with the complex *HOXA* locus. The *HOXA* cluster contains an active multi-canyon component (*HOXA7–10*; H3K27ac marked) flanked by two repressed components (Figure 7B, H3K27me3) with which the GLS interacts. The active *HOX* genes become repressed as HSPCs differentiate. The active canyons bear correctly oriented CTCF motifs consistent with extrusion loops between active *HOXA* segments (Figures 7A and 7B). The Hi-C data and epigenomic profile suggest the *HOXA9* region forms a 3D genomic structure, modeled in Figure 7H. Thus, we hypothesized that the GLS and repressed *HOXA* interactions would be important for HSC function.

To test this, we deleted the GLS in HSPCs (Gundry et al., 2016) and compared these with unedited wild-type (WT) HSPCs (Figure 7C; Figure S7A). The deletion efficiency of the ~17 kb GLS was estimated at about 50% (Figure 7C). To determine if GLS deletion affected self-renewal and differentiation, we used digital droplet PCR (ddPCR) to quantify the edited and unedited HSPCs in the CD34+ CD38– versus CD34+CD38+ (more differentiated) fractions (Figure 7D). Cells with GLS deletion were enriched in the more differentiated population (Figure 7E), suggesting maintenance of the GLS is associated with stem cell identity.

Because high H3K27me3 is critical for maintaining grand canyon interactions, we asked if its modulation would hinder the GLS-HOXA interaction and alter gene expression. We treated HSPCs with the EZH2 inhibitor and found that H3K27me3 was reduced at the GLS locus. Although the GLS-HOXA interaction became attenuated in the *ex vivo* expanded HSPCs, it was further disrupted in the presence of the EZH2 inhibitor, as seen using Hi-C (Figure 7F). Concomitantly, *HOXA9*

Figure 4. DNA Methylation Canyons Are Long Loop Anchors

- (A) Example of HiCCUPS loops and long loops on chromosome 2. Blue dots represent long loops and green dots represent HiCCUPS loops. The matrices are shown at 100 kb resolution and blow out of *POU3F3*, *HOXD*, and *PAX3* regions at 5 kb resolution. Green bars represent DNA methylation canyons.
- (B) Example of long loops on chromosome 6 convergent on grand canyon regions. The matrices are shown at 100 kb resolution and blowout of *POUF2*, *PRDM13*, and *SIM1* regions at 5 kb resolution.
- (C) Example of long loops on chromosome 7 with grand canyons. The matrices are shown at 100 kb resolution of *TWIST1*, *SP8*, and *HOXA11-EVX1* regions.
- (D) Fold enrichment of grand canyons at loop anchors (HiCCUPS loops, blue bars; long loops, red bar).
- (E) Upper panel: the enrichment of H3K27ac and H3K27me3 in the grand canyon region. Lower panel: the comparison of ChIP-seq signal of H3K27ac and H3K27me3 in grand canyon region (>7.3 kb), short canyon region (3.5–7.3 kb), UMRs between 3.5 and 1 kb, and UMRs less than 1 kb. UMR, under-methylated region.
- (F) The aggregated peak analysis (APA) on grand canyon interactions, with different length scale and inter-chromosomal interactions in HSPCs. Loop interactions are shown as a control. RGC, repressive grand canyons; srUMR, short repressive UMR. srUMRs are UMRs shorter than 3.5 kb and enriched for H3K27me3 signal. HMEC, human primary epithelial mammary cell.

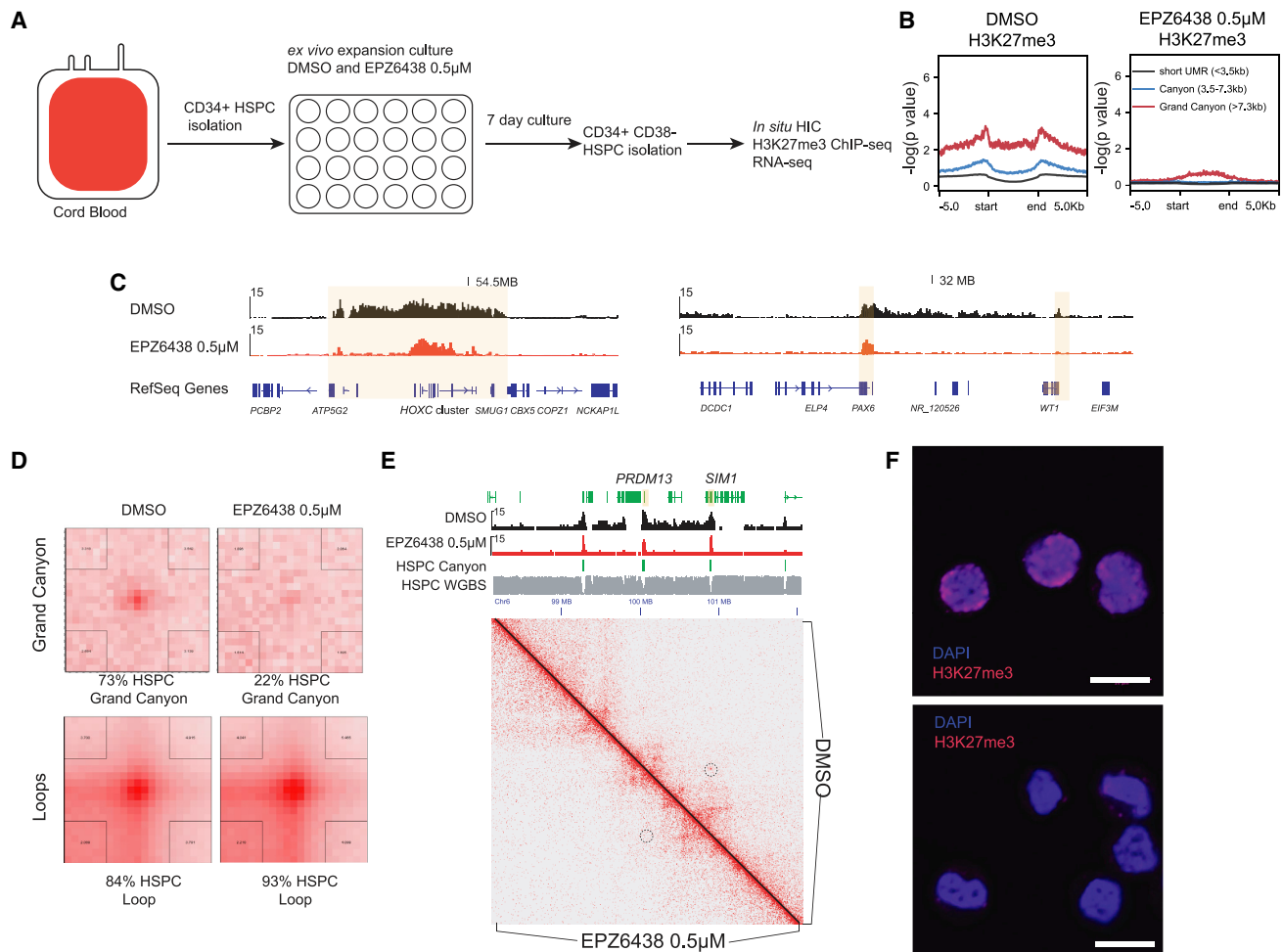


Figure 5. Grand Canyon Interactions Require High H3K27me3 Deposited by EZH2

(A) The experimental scheme. Cord blood CD34+ cells are treated with EZH2 inhibitor for 7 days in the *ex vivo* culture condition. The CD34+CD38- cells are isolated for *in situ* Hi-C, RNA sequencing (RNA-seq), and ChIP-seq.

(B) Level of global H3K27me3 ChIP-seq signal on CD34+CD38- cells after vehicle and EZH2 inhibitor treatment for 7 days. MACS2 enrichment fold change is shown on the y axis.

(C) H3K27me3 enrichment on CD34+CD38- cells around HOXC cluster and PAX6-WT1 locus after vehicle and EZH2 inhibitor treatment for 7 days.

(D) APA on grand canyon interactions and CTCF loops in vehicle and EZH2 inhibitor treatment cells.

(E) Example of grand canyon interaction loss in EZH2 inhibitor-treated cells in *PRDM13* and *SIM1*.

(F) Immunostaining of H3K27me3 in DMSO and EZH2 inhibitor-treated cells. Scale bar, 10 μ m. Representative image is displayed with the same exposure time.

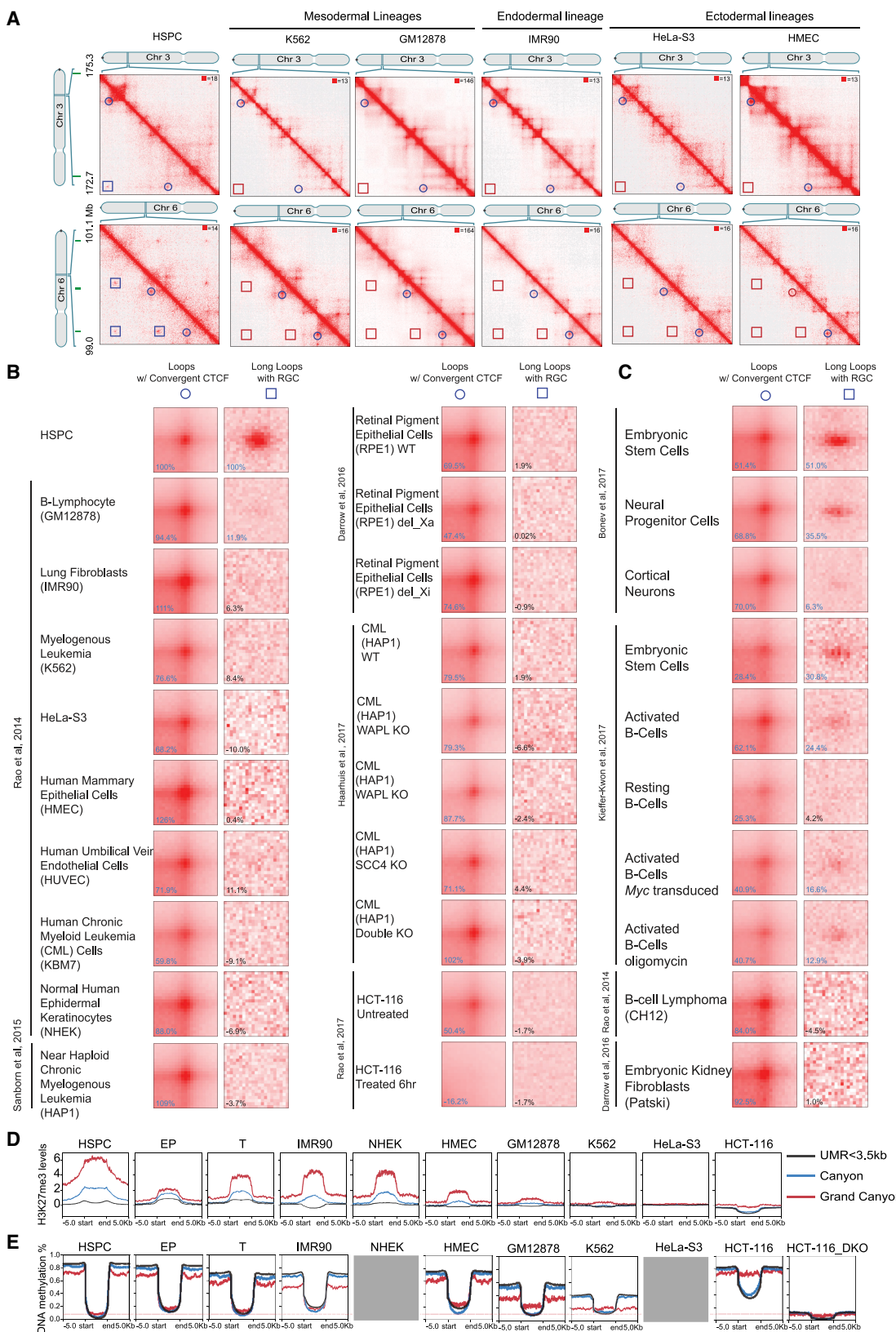
expression significantly decreased by almost 2-fold (Figure 7G), while the previously repressed *HOXA11* gene became activated after EZH2 inhibitor treatment. These data support the concept that the H3K27me3 interactions in the GLS and HOXA canyons are maintaining, rather than repressing, appropriate gene expression at this locus.

In summary, the genetic and epigenetic modulation of the GLS-HOXA interactions support the concept that the GLS-HOXA canyons support a superstructure that enables expression of stem cell-associated transcription factors *HOXA9/10* in HSCs. We speculate that this represents a dedicated 3D structure that connects enhancers to the active HOXA genes (Figure 7H). Disruption of the GLS-HOXA canyon interaction results in decreased expression of active HOXA genes.

DISCUSSION

Here we describe a unique class of very long loops that are frequently anchored at DNA methylation canyons bearing histones with the highest levels of the repressive H3K27me3 mark. These loops are highly enriched in stem and progenitor cells, including embryonic stem cells, neural stem cells, and HSPCs. Deletion of one particular repressed grand canyon demonstrated a functional association with HSPC multipotency.

These long loops differ from those previously observed in several aspects: (1) they bind CTCF much less frequently, (2) they do not respect the CTCF convergent rule, and (3) their anchors form links at arbitrary distances and across different chromosomes. In all of these aspects, the long loops and links we



(legend on next page)

report here are similar to those between super-enhancers (Beagrie et al., 2017; Rao et al., 2017; Sabari et al., 2018). However, they differ in two key ways: (1) the loops and links in HSPCs connect repressed DNA methylation canyons, rather than active regions, and (2) they form in primary cells under physiological conditions.

Recently, we proposed that some loops form via cohesin-associated extrusion, whereas others form by compartmentalization (Rao et al., 2014, 2017; Sanborn et al., 2015). Loop extrusion is restricted to pairs of loci on the same chromosome, whereas compartmentalization can occur between chromosomes. The grand canyon interactions here appear distinct from the B1 subcompartment. In aggregate, grand canyons only span \sim 3.5 Mb, or roughly 0.1% of the human genome, and are more enriched in H3K27me3 than other regions of the genome (Figure 4E). The B1 subcompartment covers a much larger portion of the genome (\sim 400 Mb) (Rao et al., 2014). Although Polycomb has also been implicated in some long-range interactions in embryonic stem cells (Bonev et al., 2017), these were associated with RING1B binding and showed a low association with H3K27me3. Furthermore, from Epigenome Roadmap data (Kundaje et al., 2015), we estimate the entire H3K27me3-covered region in human HSPCs to be on the order of 655 Mb. Therefore, the grand canyons that anchor the long loops we are describing represent a tiny subset of the genome that is marked by the highest levels of H3K27me3.

Megabase-size loops have been described in some other studies. The transcription factor LHX1 has been shown to regulate long-range interactions in the context of olfactory receptor expression (Monahan et al., 2019). Similarly, a \sim 2.8 Mb interaction is associated with MYC activation by a super-enhancer (Schuijers et al., 2018). Both of these cases represent interactions between active rather than repressed loci.

Taken together, our data pinpoint sites of very-long-range loops that represent a class of interactions specific to primary stem and progenitor cells. The absence of such interactions in cell lines suggests that tissue culture can affect grand canyon interactions (Figure 5D), but we cannot exclude interactions that improved bioinformatic tools may uncover.

A Phase Separation-like Nature for Grand Canyon Interactions

These long loops are consistent with a model in which repressed grand canyons tend to co-segregate with multiple anchors simultaneously. Recently, co-segregation of active regions has been proposed to occur as a consequence of phase separation (Hnisz et al., 2017; Larson et al., 2017; Rowley et al., 2017; Strom

et al., 2017). Our analysis indicated that the most distant interactions were between canyons exhibiting the highest H3K27me3 signals, suggesting that critical levels of H3K27me3 may be required to segregate together and into long-range interactions. This concept is supported by the EZH2 inhibitor treatment, which led to reduced H3K27me3 and loss of long loops. Together, the H3K27me3 concentration dependence for the long-range interactions is consistent with a phase separation nature (Alberti, 2017), a concept supported by other studies (Lorzadeh et al., 2016; Xu et al., 2018).

Polycomb proteins have previously been shown to exhibit liquid-liquid phase separation features by forming condensates mediated by CBX2 or by SAM-domain polymerization of PHC2 (Isono et al., 2013; Pirrotta and Li, 2012; Tatavosian et al., 2019). In the classic Polycomb model, PRC1 proteins such as RING1B are recruited by H3K27me3. Thus, an alternative explanation for our data is that high levels of H3K27me3 recruit high levels of PRC1 components such as RING1B that in turn form condensate foci (Isono et al., 2013) when a critical concentration is reached.

The Role of DNA Methylation in Grand Canyon Interactions

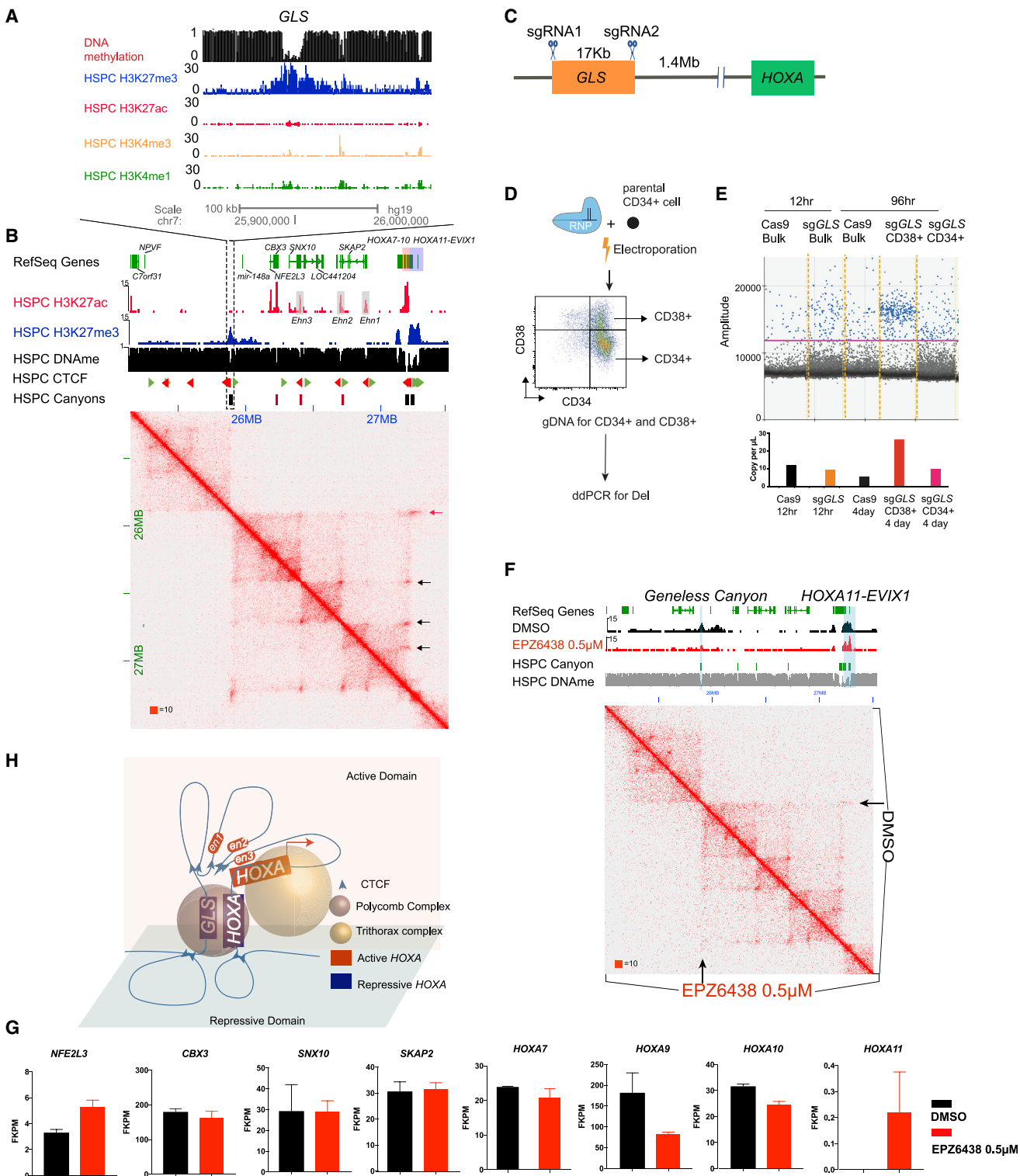
The alignment of the sharply delineated DNA methylation canyons with long distance contacts is striking. We propose that DNA methylation nadirs enable distal interactions in part by guiding precise deposition of histone marks that mediate the genomic interactions. The DNA methylation patterns are maintained by competing DNMT3A and TET protein activity (Gu et al., 2018; Jeong et al., 2014; Zhang et al., 2016), which serve to restrict the boundary of these regions. Our data show that DNA methylation demarcates regions with the highest levels of H3K27me3. Consistent with this role for DNA methylation is the recent observations that DNA methylation is required for the Polycomb-associated interaction in embryonic stem cells (McLaughlin et al., 2019).

Interestingly, *Drosophila* Hox genes, when repressed by Polycomb, have been shown to interact at a distance (Bantignies et al., 2011; Boettiger et al., 2016). Although *Drosophila* lack DNA methylation, they have Polycomb response elements (PREs) that enable formation of well-demarcated Polycomb domains. We speculate that the sharp DNA methylation transitions at canyons may enable very high localized Polycomb concentrations, analogous to role of the PRE.

If DNA methylation is important, how do DNA methylation changes affect these higher-order interactions? Human cell lines used in all early Hi-C studies lack these long-range interactions

Figure 6. Canyon Interactions Are Strongly Enriched in Undifferentiated Cell Types

- (A) Example of HICCUPS loops (circles) and long loops (squares) on chromosomes 3 and 6 across cell types (left). APA for loops with convergent CTCF and long loops with repressive grand canyons across cell types (right). Canyons are indicated in green (top).
- (B) APA on the indicated human cell types.
- (C) APA on the indicated mouse cell types.
- (D) Levels of H3K27me3 in the grand canyon, canyon, and UMRs $<$ 3.5 kb in cells with both Hi-C data and H3K27me3 in (B) (H3K27me3ChIP-input). FPKM (fragments per kilobase of transcript per million mapped reads) value from deepTools 2.0 is shown on the y axis. H3K27me3 data are from ENCODE, listed in STAR Methods.
- (E) Levels of DNA methylation in the grand canyon, canyon, and UMRs $<$ 3.5 kb in cells with both Hi-C data and whole-genome bisulfite sequencing (WGBS) data in (B). DNA methylation level value is shown on the y axis. The red line indicates the methylation level of grand canyon in HSPC. Gray box indicates that the corresponding DNA methylation data are not available through ENCODE.

**Figure 7. HOXA Long-Range Interactions Maintain HSPC Identity**

(A) Epigenome browser track image of the geneless (GLS) canyon between the *MIR148A* and the *RNU6-16P* locus. H3K4me3, H3K27me3, H3K27ac, H3K4me1, CTCF orientation, and DNA methylation are displayed for HSPCs. Green arrowheads indicate the reverse CTCF, and red arrowheads indicate the forward CTCF sites.

(legend continued on next page)

and are known to exhibit aberrant DNA methylation patterns (Jones, 2012; Jones and Baylin, 2002). Moreover, modest DNA methylation increases at canyons in differentiated erythroid and T cells are accompanied by a loss of the canyon-canyon interactions. Whether DNA methylation changes alter canyon-canyon interactions needs to be determined.

It is also possible that DNA methylation changes affect long-range through known mechanisms, such as changing the affinity of binding of DNA methylation-sensitive transcription factors (Hashimoto et al., 2016; Lewis and Bird, 1991) or of CTCF (Bell and Felsenfeld, 2000; Hark et al., 2000; Hashimoto et al., 2017). Changes in DNA methylation may affect chromatin organization through multiple non-exclusive mechanisms.

Grand Canyon Interactions Regulate HOXA Cluster Gene Expression in HSPCs

The importance of appropriate HOXA locus expression for HSPCs is well established (Di-Poï et al., 2010; Soshnikova et al., 2013). In particular, HOXA9 and HOXA10 are highly expressed in HSPCs, are important for self-renewal, and are commonly dysregulated in acute myeloid leukemia (AML) (Spencer et al., 2015), in which they maintain a stem cell-like state. EZH2 inhibitor treatment led to reduced canyon-canyon interactions and alterations in HOX expression, suggesting that repressed domains can be important for distal gene expression, analogous to role of enhancers. One possible model is that the repressive domains provide a scaffold that enables appropriate HOXA expression (Figure 7H). We propose that Polycomb domains, together with local nuclear structure, allow a 3D structure that segments the HOXA locus, ensuring stable appropriate HOXA gene expression. The concept of spatially proximate active and repressive domains has some precedent in embryonic stem cells and *Drosophila* (Barbieri et al., 2017; Cattoni et al., 2017), but the importance of the repressive domains for appropriate activity of linked regions has not been established.

The GLS represents a heretofore unknown putative regulatory element of the HOXA locus. The mouse GLS homolog has recently been implicated in limb development, also through a proposed interaction between the repressive domain with the *HoxA* region (Gentile et al., 2019). Although most canyons includes the promoter of a protein-coding gene, some, such as the GLS, are upstream of known genes. Importantly, canyon marks are cell type specific: canyons may bear active or repressive marks depending on the cell type (Jeong et al., 2014). Therefore, the GLS may be active, perhaps as an enhancer, in some contexts (Figure S7B). Given that super-enhancers, which over-

lap with active canyons when active (Jeong et al., 2014), participate in nuclear condensates (Sabari et al., 2018), and PRC domains are also implicated in a distinct phase, canyons may represent elements that can switch between different types of nuclear condensates.

In summary, we show here that DNA methylation grand canyons represent an important genome element that mediate chromatin looping when decorated with H3K27me3. Rather than forming by extrusion, these loops are likely to form by compartmentalization. These loops and links are enriched in stem and progenitor cells, diminishing as cells differentiate. These findings coalesce observations from several other studies and illuminate the role of DNA methylation in the genome.

STAR★METHODS

Detailed methods are provided in the online version of this paper and include the following:

- **KEY RESOURCES TABLE**
- **RESOURCE AVAILABILITY**
 - Lead Contact
 - Materials Availability
 - Data and Code Availability
- **EXPERIMENTAL MODEL AND SUBJECT DETAILS**
 - HSPCs, T cells and erythroid progenitors
- **METHOD DETAILS**
 - *In situ* Hi-C library construction and data analysis
 - CRISPR-mediated deletion in CD34+ cells
 - EZH2 inhibitor treatment
 - Whole genome bisulfite sequencing (WGBS) and analysis
 - Canyon Identification
 - DNA FISH
 - ChIP-sequencing (ChIP-seq)
 - CTCF occupancy and orientation
 - RNA-Seq
 - Aggregated peak analysis (APA) of canyon interaction
 - APA analysis on published Hi-C data
 - Cross sample H3K27me3 ChIP-seq analysis and data visualization

SUPPLEMENTAL INFORMATION

Supplemental Information can be found online at <https://doi.org/10.1016/j.molcel.2020.04.018>.

(B) Contact matrices of GLS and HOXA cluster region on chromosome 7 at 5 kb resolution in CD34+ HSPCs. Red squares, canyons; black squares, grand canyons. Black arrow indicates the interaction between active HOXA genes with upstream H3K27ac marked enhancers. Red arrow indicates grand canyon interactions of GLS and repressive HOXA regions.

(C) Schematic representation of CRISPR-Cas9 targeting of the geneless (GLS) canyon.

(D) Scheme for testing the role of GLS in HSPC maintenance by CRISPR-Cas9 deletion of GLS in HSPC.

(E) ddPCR quantification of GLS deletion band.

(F) Interaction in GLS-HOXA locus after EZH2 inhibitor treatment (lower triangle) in comparison with DMSO (upper triangle) in ex vivo culture system from CD34+ CD38- HSPCs; H3K27me3 ChIP-seq is shown on top. Blue shade indicates the site of GLS and HOXA. Arrow points to GLS-HOXA interaction in HSPCs.

(G) FPKM value of genes between HOXA cluster and GLS after EZH2 inhibitor treatment in ex vivo culture system from CD34+ CD38- HSPCs. n = 2 in each treatment.

(H) Three-dimensional model of genomic interactions between GLS and HOXA.

ACKNOWLEDGMENTS

This work was supported by NIH grants CA125123, 1DP2OD008540, HG007538, CA228140, DK092883, DK56338, CA183252, 5T32DK60445, U01HL130010, UM1HG009375, ES030285, and 1S10OD023469 and the Samuel Waxman Cancer Research Foundation Investigator. This work was also supported by the National Science Foundation (NSF) (PHY-1427654), the Welch Foundation (Q-1866), an Nvidia Research Award, an IBM University Challenge Award, a Google Research Award, the Cancer Prevention Research Institute of Texas (R1304, RP180672, RR024574, RP150578, and RP170719), the McNair Medical Institute, and the President's Early Career Award in Science and Engineering. X.Z. is supported by the American Society of Hematology, the EvansMDS Foundation, and a VAR! fellowship. We also thank Dr. Xudong Wu (Tianjin Medical University) and Dr. Fei Lan (Fudan University) for helpful discussions.

AUTHOR CONTRIBUTIONS

Conceptualizations, X.Z., M.J., X.H., M.A.G., and E.L.A.; Methodology, M.J., H.G., P.H., Y.L., X.Z., A.P.A., W.L., and I.D.B.; Analysis, M.S.S., X.H., X.W., W.Z., P.H., J.S., X.Q.W., M.D., Y.-H.H., and J.R.; Investigation, M.J., X.H., X.Z., H.J., X.Q.W., and E.H.; Writing & Editing, X.Z., M.J., X.H., X.W., X.Q.W., E.L.A., J.S., and M.A.G.; Supervision, X.Z., E.L.A., and M.A.G.

DECLARATION OF INTERESTS

The authors declare no competing interests.

Received: October 19, 2019

Revised: January 6, 2020

Accepted: April 15, 2020

Published: May 7, 2020

REFERENCES

Alberti, S. (2017). Phase separation in biology. *Curr. Biol.* 27, R1097–R1102.

Alipour, E., and Marko, J.F. (2012). Self-organization of domain structures by DNA-loop-extruding enzymes. *Nucleic Acids Res.* 40, 11202–11212.

Bantignies, F., Roure, V., Comet, I., Leblanc, B., Schuettengruber, B., Bonnet, J., Tixier, V., Mas, A., and Cavalli, G. (2011). Polycomb-dependent regulatory contacts between distant Hox loci in *Drosophila*. *Cell* 144, 214–226.

Barbieri, M., Xie, S.Q., Torlai Triglia, E., Chiariello, A.M., Bianco, S., de Santiago, I., Branco, M.R., Rueda, D., Nicodemi, M., and Pombo, A. (2017). Active and poised promoter states drive folding of the extended HoxB locus in mouse embryonic stem cells. *Nat. Struct. Mol. Biol.* 24, 515–524.

Beagrie, R.A., Scialdone, A., Schueler, M., Kraemer, D.C., Chotalia, M., Xie, S.Q., Barbieri, M., de Santiago, I., Lavitas, L.M., Branco, M.R., et al. (2017). Complex multi-enhancer contacts captured by genome architecture mapping. *Nature* 543, 519–524.

Bell, A.C., and Felsenfeld, G. (2000). Methylation of a CTCF-dependent boundary controls imprinted expression of the *Igf2* gene. *Nature* 405, 482–485.

Bird, A., Taggart, M., Frommer, M., Miller, O.J., and Macleod, D. (1985). A fraction of the mouse genome that is derived from islands of nonmethylated, CpG-rich DNA. *Cell* 40, 91–99.

Boettiger, A.N., Bantu, B., Moffitt, J.R., Wang, S., Beliveau, B.J., Fudenberg, G., Imakaev, M., Mirny, L.A., Wu, C.T., and Zhuang, X. (2016). Super-resolution imaging reveals distinct chromatin folding for different epigenetic states. *Nature* 529, 418–422.

Bonev, B., Mendelson Cohen, N., Szabo, Q., Fritsch, L., Papadopoulos, G.L., Lubling, Y., Xu, X., Lv, X., Hugnot, J.P., Tanay, A., et al. (2017). Multiscale 3D genome rewiring during mouse neural development. *Cell* 171, 557–572.e24.

Cattoni, D.I., Cardozo-Gizzi, A.M., Georgieva, M., Di Stefano, M., Valeri, A., Chamouset, D., Houbron, C., Dejardin, S., Fiche, J.-B., Marti-Renom, M.A., et al. (2017). Single-cell absolute contact probability detection reveals that chromosomes are organized by modulated stochasticity. *bioRxiv*. <https://doi.org/10.1101/159814>.

Challen, G.A., Sun, D., Jeong, M., Luo, M., Jelinek, J., Berg, J.S., Bock, C., Vasanthakumar, A., Gu, H., Xi, Y., et al. (2011). Dnmt3a is essential for hematopoietic stem cell differentiation. *Nat. Genet.* 44, 23–31.

Choi, J.W., Lee, S.Y., and Choi, Y. (1996). Identification of a putative G protein-coupled receptor induced during activation-induced apoptosis of T cells. *Cell. Immunol.* 168, 78–84.

Cullen, K.E., Kladde, M.P., and Seyfried, M.A. (1993). Interaction between transcription regulatory regions of prolactin chromatin. *Science* 261, 203–206.

Darrow, E.M., Huntley, M.H., Dudchenko, O., Stamenova, E.K., Durand, N.C., Sun, Z., Huang, S.C., Sanborn, A.L., Machol, I., Shamim, M., et al. (2016). Deletion of DXZ4 on the human inactive X chromosome alters higher-order genome architecture. *Proc. Natl. Acad. Sci. U S A* 113, E4504–E4512.

Di-Poï, N., Koch, U., Radtke, F., and Duboule, D. (2010). Additive and global functions of HoxA cluster genes in mesoderm derivatives. *Dev. Biol.* 341, 488–498.

Dixon, J.R., Selvaraj, S., Yue, F., Kim, A., Li, Y., Shen, Y., Hu, M., Liu, J.S., and Ren, B. (2012). Topological domains in mammalian genomes identified by analysis of chromatin interactions. *Nature* 485, 376–380.

Dixon, J.R., Jung, I., Selvaraj, S., Shen, Y., Antosiewicz-Bourget, J.E., Lee, A.Y., Ye, Z., Kim, A., Rajagopal, N., Xie, W., et al. (2015). Chromatin architecture reorganization during stem cell differentiation. *Nature* 518, 331–336.

Durand, N.C., Robinson, J.T., Shamim, M.S., Machol, I., Mesirov, J.P., Lander, E.S., and Aiden, E.L. (2016a). Juicebox provides a visualization system for Hi-C contact maps with unlimited zoom. *Cell Syst.* 3, 99–101.

Durand, N.C., Shamim, M.S., Machol, I., Rao, S.S., Huntley, M.H., Lander, E.S., and Aiden, E.L. (2016b). Juicer provides a one-click system for analyzing loop-resolution Hi-C experiments. *Cell Syst.* 3, 95–98.

Fudenberg, G., Imakaev, M., Lu, C., Goloborodko, A., Abdennur, N., and Mirny, L.A. (2016). Formation of chromosomal domains by loop extrusion. *Cell Rep.* 15, 2038–2049.

Gentile, C., Berlivet, S., Mayran, A., Paquette, D., Guerard-Millet, F., Bajon, E., Dostie, J., and Kmita, M. (2019). PRC2-associated chromatin contacts in the developing limb reveal a possible mechanism for the atypical role of PRC2 in HoxA gene expression. *Dev. Cell* 50, 184–196.e4.

Gu, T., Lin, X., Cullen, S.M., Luo, M., Jeong, M., Esteceo, M., Shen, J., Hardikar, S., Sun, D., Su, J., et al. (2018). DNMT3A and TET1 cooperate to regulate promoter epigenetic landscapes in mouse embryonic stem cells. *Genome Biol.* 19, 88.

Gundry, M.C., Brunetti, L., Lin, A., Mayle, A.E., Kitano, A., Wagner, D., Hsu, J.I., Hoegneauer, K.A., Rooney, C.M., Goodell, M.A., and Nakada, D. (2016). Highly efficient genome editing of murine and human hematopoietic progenitor cells by CRISPR/Cas9. *Cell Rep.* 17, 1453–1461.

Haarhuis, J.H.I., van der Weide, R.H., Blomen, V.A., Yanez-Cuna, J.O., Amendola, M., van Ruiten, M.S., Krijger, P.H.L., Teunissen, H., Medema, R.H., van Steensel, B., et al. (2017). The cohesin release factor WAPL restricts chromatin loop extension. *Cell* 169, 693–707.e14.

Hark, A.T., Schoenherr, C.J., Katz, D.J., Ingram, R.S., Levorse, J.M., and Tilghman, S.M. (2000). CTCF mediates methylation-sensitive enhancer-blocking activity at the H19/Igf2 locus. *Nature* 405, 486–489.

Hashimoto, H., Wang, D., Steves, A.N., Jin, P., Blumenthal, R.M., Zhang, X., and Cheng, X. (2016). Distinctive Klf4 mutants determine preference for DNA methylation status. *Nucleic Acids Res.* 44, 10177–10185.

Hashimoto, H., Wang, D., Horton, J.R., Zhang, X., Corces, V.G., and Cheng, X. (2017). Structural basis for the versatile and methylation-dependent binding of CTCF to DNA. *Mol. Cell* 66, 711–720.e3.

Hnisz, D., Shrinivas, K., Young, R.A., Chakraborty, A.K., and Sharp, P.A. (2017). A phase separation model for transcriptional control. *Cell* 169, 13–23.

Isono, K., Endo, T.A., Ku, M., Yamada, D., Suzuki, R., Sharif, J., Ishikura, T., Toyoda, T., Bernstein, B.E., and Koseki, H. (2013). SAM domain polymerization links subnuclear clustering of PRC1 to gene silencing. *Dev. Cell* 26, 565–577.

Jeong, M., Sun, D., Luo, M., Huang, Y., Challen, G.A., Rodriguez, B., Zhang, X., Chavez, L., Wang, H., Hannah, R., et al. (2014). Large conserved domains of low DNA methylation maintained by Dnmt3a. *Nat. Genet.* 46, 17–23.

Jones, P.A. (2012). Functions of DNA methylation: islands, start sites, gene bodies and beyond. *Nat. Rev. Genet.* 13, 484–492.

Jones, P.A., and Baylin, S.B. (2002). The fundamental role of epigenetic events in cancer. *Nat. Rev. Genet.* 3, 415–428.

Kieffer-Kwon, K.R., Nimura, K., Rao, S.S.P., Xu, J., Jung, S., Pekowska, A., Dose, M., Stevens, E., Mathe, E., Dong, P., et al. (2017). Myc regulates chromatin decompaction and nuclear architecture during B cell activation. *Mol. Cell* 67, 566–578.e10.

Kim, T., Seo, H.D., Hennighausen, L., Lee, D., and Kang, K. (2018). Octopus-toolkit: a workflow to automate mining of public epigenomic and transcriptomic next-generation sequencing data. *Nucleic Acids Res.* 46, e53.

Kundaje, A., Meuleman, W., Ernst, J., Bilenky, M., Yen, A., Heravi-Moussavi, A., Kheradpour, P., Zhang, Z., Wang, J., Ziller, M.J., et al.; Roadmap Epigenomics Consortium (2015). Integrative analysis of 111 reference human epigenomes. *Nature* 518, 317–330.

Langmead, B., and Salzberg, S.L. (2012). Fast gapped-read alignment with Bowtie 2. *Nat. Methods* 9, 357–359.

Larson, A.G., Elnatan, D., Keenen, M.M., Trnka, M.J., Johnston, J.B., Burlingame, A.L., Agard, D.A., Redding, S., and Narlikar, G.J. (2017). Liquid droplet formation by HP1 α suggests a role for phase separation in heterochromatin. *Nature* 547, 236–240.

Lewis, J., and Bird, A. (1991). DNA methylation and chromatin structure. *FEBS Lett.* 285, 155–159.

Lieberman-Aiden, E., van Berkum, N.L., Williams, L., Imakaev, M., Ragoczy, T., Telling, A., Amit, I., Lajoie, B.R., Sabo, P.J., Dorschner, M.O., et al. (2009). Comprehensive mapping of long-range interactions reveals folding principles of the human genome. *Science* 326, 289–293.

Lorzadeh, A., Bilenky, M., Hammond, C., Knapp, D.J.H.F., Li, L., Miller, P.H., Carles, A., Heravi-Moussavi, A., Gakkhar, S., Moksa, M., et al. (2016). Nucleosome density ChIP-Seq identifies distinct chromatin modification signatures associated with MNase accessibility. *Cell Rep.* 17, 2112–2124.

Luo, M., Jeong, M., Sun, D., Park, H.J., Rodriguez, B.A., Xia, Z., Yang, L., Zhang, X., Sheng, K., Darlington, G.J., Li, W., and Goodell, M.A. (2015). Long non-coding RNAs control hematopoietic stem cell function. *Cell Stem Cell* 16, 426–438.

Madzo, J., Liu, H., Rodriguez, A., Vasanthakumar, A., Sundaravel, S., Caces, D.B.D., Looney, T.J., Zhang, L., Lepore, J.B., Macrae, T., et al. (2014). Hydroxymethylation at gene regulatory regions directs stem/early progenitor cell commitment during erythropoiesis. *Cell Rep.* 6, 231–244.

McLaughlin, K., Flyamer, I.M., Thomson, J.P., Mjoseng, H.K., Shukla, R., Williamson, I., Grimes, G.R., Illingworth, R.S., Adams, I.R., Pennings, S., et al. (2019). DNA methylation directs Polycomb-dependent 3D genome re-organization in naïve pluripotency. *Cell Rep.* 29, 1974–1985.e6.

Monahan, K., Horta, A., and Lomvardas, S. (2019). LHX2- and LDB1-mediated trans interactions regulate olfactory receptor choice. *Nature* 565, 448–453.

Nasmyth, K. (2001). Disseminating the genome: joining, resolving, and separating sister chromatids during mitosis and meiosis. *Annu. Rev. Genet.* 35, 673–745.

Nichols, M.H., and Corces, V.G. (2015). A CTCF code for 3D genome architecture. *Cell* 162, 703–705.

Nora, E.P., Goloborodko, A., Valton, A.L., Gibcus, J.H., Uebersohn, A., Abdennur, N., Dekker, J., Mirny, L.A., and Bruneau, B.G. (2017). Targeted degradation of CTCF decouples local insulation of chromosome domains from genomic compartmentalization. *Cell* 169, 930–944.e22.

Pirrotta, V., and Li, H.B. (2012). A view of nuclear Polycomb bodies. *Curr. Opin. Genet. Dev.* 22, 101–109.

Ramírez, F., Dündar, F., Diehl, S., Grüning, B.A., and Manke, T. (2014). deepTools: a flexible platform for exploring deep-sequencing data. *Nucleic Acids Res.* 42, W187–W191.

Rao, S.S., Huntley, M.H., Durand, N.C., Stamenova, E.K., Bochkov, I.D., Robinson, J.T., Sanborn, A.L., Machol, I., Omer, A.D., Lander, E.S., and Aiden, E.L. (2014). A 3D map of the human genome at kilobase resolution reveals principles of chromatin looping. *Cell* 159, 1665–1680.

Rao, S.S.P., Huang, S.C., Glenn St Hilaire, B., Engreitz, J.M., Perez, E.M., Kieffer-Kwon, K.R., Sanborn, A.L., Johnstone, S.E., Bascom, G.D., Bochkov, I.D., et al. (2017). Cohesin loss eliminates all loop domains. *Cell* 171, 305–320.e24.

Rowley, M.J., Nichols, M.H., Lyu, X., Ando-Kuri, M., Rivera, I.S.M., Hermetz, K., Wang, P., Ruan, Y., and Corces, V.G. (2017). Evolutionarily conserved principles predict 3D chromatin organization. *Mol. Cell* 67, 837–852.e7.

Sabari, B.R., Dall'Agnese, A., Boija, A., Klein, I.A., Coffey, E.L., Shrinivas, K., Abraham, B.J., Hannett, N.M., Zamudio, A.V., Manteiga, J.C., et al. (2018). Coactivator condensation at super-enhancers links phase separation and gene control. *Science* 361, eaar3958.

Sanborn, A.L., Rao, S.S., Huang, S.C., Durand, N.C., Huntley, M.H., Jewett, A.I., Bochkov, I.D., Chinnappan, D., Cutkosky, A., Li, J., et al. (2015). Chromatin extrusion explains key features of loop and domain formation in wild-type and engineered genomes. *Proc. Natl. Acad. Sci. U S A* 112, E6456–E6465.

Schuijers, J., Manteiga, J.C., Weintraub, A.S., Day, D.S., Zamudio, A.V., Hnisz, D., Lee, T.I., and Young, R.A. (2018). Transcriptional dysregulation of MYC reveals common enhancer-docking mechanism. *Cell Rep.* 23, 349–360.

Sneeringer, C.J., Scott, M.P., Kuntz, K.W., Knutson, S.K., Pollock, R.M., Richon, V.M., and Copeland, R.A. (2010). Coordinated activities of wild-type plus mutant EZH2 drive tumor-associated hypertrimethylation of lysine 27 on histone H3 (H3K27) in human B-cell lymphomas. *Proc. Natl. Acad. Sci. U S A* 107, 20980–20985.

Soshnikova, N., Dewaele, R., Janvier, P., Krumlauf, R., and Duboule, D. (2013). Duplications of hox gene clusters and the emergence of vertebrates. *Dev. Biol.* 378, 194–199.

Spencer, D.H., Young, M.A., Lamprecht, T.L., Helton, N.M., Fulton, R., O'Laughlin, M., Fronick, C., Magrini, V., Demeter, R.T., Miller, C.A., et al. (2015). Epigenomic analysis of the HOX gene loci reveals mechanisms that may control canonical expression patterns in AML and normal hematopoietic cells. *Leukemia* 29, 1279–1289.

Strom, A.R., Emelyanov, A.V., Mir, M., Fyodorov, D.V., Darzacq, X., and Karpen, G.H. (2017). Phase separation drives heterochromatin domain formation. *Nature* 547, 241–245.

Sun, D., Xi, Y., Rodriguez, B., Park, H.J., Tong, P., Meong, M., Goodell, M.A., and Li, W. (2014). MOABS: model based analysis of bisulfite sequencing data. *Genome Biol.* 15, R38.

Tatavosian, R., Kent, S., Brown, K., Yao, T., Duc, H.N., Huynh, T.N., Zhen, C.Y., Ma, B., Wang, H., and Ren, X. (2019). Nuclear condensates of the Polycomb protein chromobox 2 (CBX2) assemble through phase separation. *J. Biol. Chem.* 294, 1451–1463.

Xi, Y., and Li, W. (2009). BSMAP: whole genome bisulfite sequence MAPping program. *BMC Bioinformatics* 10, 232.

Xie, W., Schultz, M.D., Lister, R., Hou, Z., Rajagopal, N., Ray, P., Whitaker, J.W., Tian, S., Hawkins, R.D., Leung, D., et al. (2013). Epigenomic analysis of multilineage differentiation of human embryonic stem cells. *Cell* 153, 1134–1148.

Xu, J., Ma, H., Jin, J., Uttam, S., Fu, R., Huang, Y., and Liu, Y. (2018). Super-resolution imaging of higher-order chromatin structures at different epigenomic states in single mammalian cells. *Cell Rep.* 24, 873–882.

Zhang, Y., Liu, T., Meyer, C.A., Eeckhoute, J., Johnson, D.S., Bernstein, B.E., Nusbaum, C., Myers, R.M., Brown, M., Li, W., and Liu, X.S. (2008). Model-based analysis of ChIP-Seq (MACS). *Genome Biol.* 9, R137.

Zhang, X., Su, J., Jeong, M., Ko, M., Huang, Y., Park, H.J., Guzman, A., Lei, Y., Huang, Y.H., Rao, A., et al. (2016). DNMT3A and TET2 compete and cooperate to repress lineage-specific transcription factors in hematopoietic stem cells. *Nat. Genet.* 48, 1014–1023.

STAR★METHODS

KEY RESOURCES TABLE

REAGENT or RESOURCE	SOURCE	IDENTIFIER
Antibodies		
CD34 Micro beads	Miltenyi Biotech	130-100-453
Human CD34-PE	BD bioscience	340699
Human CD45-FITC	BD bioscience	340664
Human CD38-APC	BD bioscience	340677
Human CD36-FITC	BD bioscience	555454
Human CD71-APC	BD bioscience	551374
Human CD235a-PE	BD bioscience	340947
H3K27ac	Abcam	Ab4729, RRID:AB_2118291
H3K27me3	Millipore	07-449, RRID:AB_310624
CTCF	Cell signaling	2899
RING1B	Gift from H. Koseki, RIKEN	N/A
Chemicals, Peptides, and Recombinant Proteins		
SCF	Peprotech	300-07
FLT3L	Peprotech	300-19
TPO	Peprotech	300-18
IL-3	Peprotech	200-03
EPO	Peprotech	100-64
SFEM II	Stem Cell Technologies	09655
Cas9 Protein	PNA bio	CP01200
Protease inhibitor cocktail	GenDepot	P3100-001
EZH2 inhibitor-EPZ6438	Selleckchem	S7128
Biological Samples		
Cord Blood	Stem Cell transplantation Group	https://www.mdanderson.org/
Critical Commercial Assays		
Truseq DNA methylation kit	Illumina	EGMK81312
Purelink Genomic DNA kit	Invitrogen	K182001
EZ DNA Methylation kit	Zymo Research	D5005
Ampure XP beads	Beckman Coulter	5067-5582
Kapa Quantification kit	Kapa Biosystem	KK4844
Nextseq Mid output	Illumina	FC-404-2001
MinElute Purification kit	QIAGEN	28006
RNeasy micro kit	QIAGEN	28006
RNase free DNase	QIAGEN	79254
Truseq Stranded mRNA kit	Illumina	RS-122-2101
TruPLEX-DNA library prep kit	Rubicon	R400406
HiScribe RNA Synthesis kit	NEB	E2040S
Deposited Data		
Raw NGS data	This Paper	GSE104579 GSE144124 GSE144126 GSE144131
Analyzed public data		
HSPC H3K27me3 ChIP-seq	Epigenome Roadmap (GSE19465)	GSM486704
EP H3K27me3 ChIP-seq	GEO	ERS227606, ERS227598

(Continued on next page)

Continued

REAGENT or RESOURCE	SOURCE	IDENTIFIER
CD3+ T cell H3K27me3 ChIP-seq	Epigenome Roadmap(GSE18927)	GSM1102787
K562 H3K27me3 ChIP-seq	ENCODE(GSE29611)	GSM733658
GM12878 H3K27me3 ChIP-seq	ENCODE(GSE29611)	GSM733758
IMR90 H3K27me3 ChIP-seq	Roadmap(GSE16256)	GSM469968
HeLa-S3 H3K27me3 ChIP-seq	ENCODE(GSE29611)	GSM733696
HMEC H3K27me3 ChIP-seq	ENCODE(GSE29611)	GSM733722
NHEK H3K27me3 ChIP-seq	ENCODE(GSE29611)	GSM733701
HCT116 H3K27me3 ChIP-seq	GEO: GSE104334	GSM2809625
ESC H3K27me3 ChIP-seq	GEO: GSE104334	GSM2809626
NPC H3K27me3 ChIP-seq	GEO: GSE99009	GSM2629941
CN H3K27me3 ChIP-seq	GEO: GSE96107	GSM2533870
Activated B cell H3K27me3 ChIP-seq	GEO: GSE96107	GSM2533888
Resting B cell H3K27me3 ChIP-seq	GEO: GSE82144	GSM2184236
GM12878 WGBS	ENCODE	ENCSR890UQO
HMEC WGBS	ENCODE	ENCSR656TQD
K562 WGBS	ENCODE	ENCSR765JPC
IMR90 WGBS	ENCODE	ENCSR888FON
HCT116 WGBS	GEO: GSE60106	GSM1465024
Experimental Models: Cell Lines		
Human Hematopoietic Stem/progenitor Cells	TMC Stem Cell transplantation Group	https://www.mdanderson.org/
Human T cells	TMC Stem Cell transplantation Group	https://www.mdanderson.org/
FISH probes		
GLC-Green-dUTP	BAC clone: RP11-1025G19	Invitrogen
Repressive HOXA-Orange-dUTP	BAC clone: RP11-598H18	Invitrogen
TWIST1-Orange-dUTP	BAC clone: RP11.C-178P2	Invitrogen
Oligonucleotides		
GLS-sgRNA-5'	ttaatacgactcaactataGGAAAAGACACAA CCGGCGTGgttttagagctagaaatgc	IDT
GLS-sgRNA-3'	ttaatacgactcaactataGGTCAGGAGGAA GGAGAACCGtttttagagctagaaatgc	IDT
GLS-del-F	TCCTACTGTGCAGTTGTATG	IDT
GLS-del-R	ATGGGATGAGCAAATGGAAATG	IDT
GLS-WT-F	GACAGAAACTTC CCA GGA TGG	IDT
GLS-WT-R	GGGTTGGTGAGATTAGCCATAAA	IDT
Software and Algorithms		
Juicer	Durand et al., 2016b	https://github.com/aidenlab/juicer/wiki
Juicebox	Durand et al., 2016a; Durand et al., 2016b	http://aidenlab.org/juicebox/
MACS2.0	Zhang et al., 2008	https://github.com/taoliu/MACS
BSMAP	Xi and Li, 2009	https://github.com/genome-vendor/bsmap
HISAT2	Kim et al., 2018	https://github.com/infphilo/hisat2
Bowtie2	Langmead and Salzberg, 2012	http://bowtie-bio.sourceforge.net/bowtie2/index.shtml
deepTools	Ramírez et al., 2014	https://deeptools.readthedocs.io/en/develop/
Trim Glore		https://www.bioinformatics.babraham.ac.uk/projects/trim_galore/
APA	This Paper (Durand et al., 2016b)	N/A

RESOURCE AVAILABILITY

Lead Contact

All materials and data are available upon request to Margaret Goodell (goodell@bcm.edu).

Materials Availability

All contact maps reported here can be explored interactively via Juicebox at <http://www.aidenlab.org/juicebox/>.

Data and Code Availability

Raw FISH and immunostaining data are deposited at Mendeley data: <https://doi.org/10.17632/y56xsrrp8.1>. Datasets generated in this study have been deposited in the Gene Expression Omnibus, numbers GEO: GSE104579, GSE144124, GSE144126, GSE144131.

EXPERIMENTAL MODEL AND SUBJECT DETAILS

HSPCs, T cells and erythroid progenitors

Human cord blood was obtained under the institutional guidelines of Baylor College of Medicine. CD34+ HSPCs were obtained as lineage negative CD34+CD38- cells, by performing magnetic enrichment for CD34+ cells using Automacs (Miltenyi Biotech) with human CD34 micro beads (Miltenyi Biotech #130-100-453) and then flow sorting for CD45-FITC (BD #340664), CD34-PE (BD #340669), and CD38-APC (BD #340677). T cells were sorted as CD3+ cells using CD45-FITC (BD #340664), CD3-APC (BD #340661). For erythroid progenitor (EP) cells, 0.5-1X10⁶ cells magnetically enriched for CD34+ were kept in SFEM II stem cell expansion medium (Stem Cell Technologies) supplemented with 50ng/mL SCF, 25ng/mL Flt3L and 50ng/mL TPO for 5 days. CD34+ CD38- HSPCs were then sorted out. Erythroid differentiation was carried out based on previous protocol ([Madzo et al., 2014](#)) with modifications. Briefly, CD34+ CD38- progenitors were cultured in 70% IMDM, 15% FBS, 15% human serum (Sigma) supplemented with 50ng/mL human SCF, 2U/mL human EPO (Invitrogen Life technologies) and 2ng/mL human IL3. Culture medium was then replaced by the same base medium with 25ng/mL SCF, 2U/mL EPO on day 3 and 10ng/mL SCF, 2U/mL EPO on day 6. CD36+ CD71+ CD235a^{hi} erythroid progenitors were sorted and then fixed in 1% of formaldehyde for 10 min and quenched in 125mM glycine for 5min. The cell pellet was then collected and stored at -80 for Hi-C library construction.

METHOD DETAILS

In situ Hi-C library construction and data analysis

In situ Hi-C libraries were generated as described in ([Rao et al., 2014](#)). Briefly, one to five million cells were crosslinked with 1% formaldehyde for 10 min at room temperature. After nuclei permeabilization, DNA was digested with MboI, and digested fragments were labeled using biotinylated d-ATP and ligated. After reverse crosslinking, ligated DNA was purified and sheared to a length of ~400 bp and biotin labeled DNA fragments were pulled down with streptavidin beads and prepped for Illumina sequencing. The final libraries were sequenced using an Illumina X Ten instrument and sequenced reads were analyzed using the Juicer pipeline ([Durand et al., 2016b](#)). We sequenced 1,125,460,828 Hi-C read pairs in HSPC cells, yielding 613,206,292 Hi-C contacts; 965,167,644 Hi-C read pairs in T cells, yielding 474,124,006 Hi-C contacts; we also sequenced 1,377,731,051 Hi-C read pairs in EP cells, yielding 855,246,973 Hi-C contacts. Loci were assigned to A and B compartments at 500 kB resolution.

Standard loops were annotated using HiCCUPS at 5kB and 10kB resolutions with default Juicer parameters. This yielded a list of 2682 loops in HSPC, 1234 loops in T cells and 1811 loops in EP.

To identify long loops, we performed visual examination with 25-100kb resolution with balanced normalization mode. We excluded loops that were within 2 Mb of the diagonal, revealing 408 long loops. Contact domains were annotated using the Arrowhead algorithm at 5kB resolution with default Juicer parameters. This yielded a list of 3079 contact domains in HSPC, 563 in T cells and 306 contact domains in EP.

Long loops could also be identified by running HiCCUPS at course resolution and using less stringent parameters, given the large size of these loops, and the fact that the HSPC Hi-C map was not extremely deep. Specifically, HiCCUPS recognized 34 of 408 long loops in this mode.

All the code used in the above steps is publicly available at (<https://github.com/theaidenlab>). The Hi-C maps can be viewed at [aidenlab.org/juicebox](http://www.aidenlab.org/juicebox) and additional resources are available at [aidenlab.org](http://www.aidenlab.org).

CRISPR-mediated deletion in CD34+ cells

Cas9 protein (PNA bio/ IDT/NEB) and *in vitro* transcribed sgRNA (NEB Hi-Scribe kit) was used to delete the geneless canyon as previously described ([Gundry et al., 2016](#)) using *in vitro* transcribed sgRNAs. 1ug Cas9 protein and a total of 1ug sgRNA were incubated

at room temperature for 15min. 2×10^5 CD34+ cells were electroporated with the Neon transfection system with R buffer. One day after electroporation, cells were taken out to assay for the deletion.

The oligos for sgRNA synthesis and Canyon deletion detection is listed below (target sequence in sgRNA is in Upper case):

GLS-sgRNA-5': ttaatacgactcaataGGAAAAGACACACCGGCGTGgttttagagctagaaatagc
GLS-sgRNA-3': ttaatacgactcaataGGTCAGGAGGAAGGAGAACGtttttagagctagaaatagc
GLS-del-F: TCCTACTGTGCAGTTGTATG
GLS-del-R': ATGGGATGAGCAAATGAAATG
GLS-WT-F: GACAGAAACTTC CCA GGA TGG
GLS-WT-R: GGGTTGGTGAGATTAGCCATAAA

Cord Blood CD34+ HSPCs were isolated as previously described and placed in the CD34+ expansion medium- SFEM medium (Stem Cell Technology) supplemented with 100ng/mL human SCF, 100ng/mL human FLT3 and 100ng/mL human TPO. One day after culture expansion, 2×10^5 cord blood CD34+ HSPC is electroporated with Cas9 RNP complex and placed into CD34+ expansion medium. 16-24hrs later, Cells are tested for the deletion of desired regions by PCR and RNA is extracted and saved for RNA-seq analysis. For the colony forming assay, CD34+ CD38- HSPC (CD34-APC, CD38-PE both from BD) is sorted and plated into 6well plate with methocult medium (StemCell Technologies #4034). Sorted live cells were crosslinked with fresh 1% formaldehyde and stored for Hi-C library preparation.

EZH2 inhibitor treatment

CD34+ cells are cultured in ex vivo expansion medium with SFEM II medium with human TPO, SCF and FLT3L (100 μ g/mL each). DMSO or 0.5 μ M EPZ-6438 was added to medium. Cells are maintained for 6-7 days. Then CD34+ CD38- cells are isolated with flow cytometry using CD34+ CD38- antibody listed above. Isolated cells are fixed with formaldehyde as described in ChIP-seq protocol for *in situ* HiC and ChIP-seq.

Whole genome bisulfite sequencing (WGBS) and analysis

WGBS was performed on EP cells purified as described above. Genomic DNA was extracted from the sorted EPs using the PureLink Genomic DNA mini kit (Invitrogen #K182001). Bisulfite conversion and purification was carried out using 100ng of genomic DNA and the EZ DNA Methylation Gold kit (Zymo Research #D5005). After bisulfite conversion, Truseq DNA Methylation kit (Illumina, #EGMK81312) was used for WGBS library preparation. Briefly, after bisulfite conversion, the DNA synthesis primers were annealed to the converted and denatured ssDNA. DNA was synthesized from the random hexamers with a terminal tag. After making di-tagged DNA Ampure XP beads (Beckman Coulter # 5067-5582) were used. Finally, illumina single-index primers were added and the library was amplified for 10 cycles at 95°C for 30 s, 55°C for 30 s, 68°C for 3 minutes. The PCR amplified final library was cleaned up using 1X Ampure XP beads and quantified using the KAPA library quantification kit (Kapa Biosystem #KK4844). Finally, 1 μ l of undiluted library was run on the tape station using D1000 screen tape (Agilent #5056-5582). Paired end 85bp sequencing was performed using Next-seq 500 mid output kit (FC-404-2001) with the illumina NextSeq platform. The software of BSMAP([Xi and Li, 2009](#)) was used to align the reads to the human genome (hg19), and the adapters and low-quality sequences were trimmed as the default threshold of BSMAP. The methylation ratio of CpGs with sequencing depth of at least 5 reads were computed using the software MOABS([Sun et al., 2014](#)). The genome-wide under-methylated regions (UMRs) were identified based on a two-state first-order hidden Markov model as described previously ([Jeong et al., 2014](#)). WGBS data for HSPCs (GSM916025) and T cells (GSM1186660) was obtained from ENCODE.

Canyon Identification

To identify HSPC DNA methylation canyons, we used a Hidden Markov Model to identify UMRs with average proportion of methylation $\leq 10\%$ and required at least 5 CpGs per kb to satisfy the permutation-based FDR 5%. UMRs of 3.5 kb or longer were defined as canyons, and those 7.5 kb or longer were defined as grand canyons.

DNA FISH

3D FISH was adapted from ([Bonev et al., 2017](#)). Briefly, HSPCs, T and EP cells were crosslinked with 1% PFA in PBS for 10 min at room temperature. After nuclei permeabilization, Chromosome FISH probes (Empiregenomics) were added to slide and sealed the coverslip with rubber cement. Cell DNA and probes were co-denatured at 72°C for 2 minutes and hybridization was performed at 42°C overnight in Thermobrite (Abbot molecular). Cells were then washed 2 min at 72°C 0.3% Igepal/0.4XSSC and 1 min at RT 0.1% Igepal/2X SSC. After washing coverslips were mounted on slides with Vectashield (Clinisciences, France). Images were taken on an API Deltavision deconvolution microscope (Applied Precision).

ChIP-sequencing (ChIP-seq)

Chromatin Immunoprecipitation (ChIP) was performed as described previously ([Luo et al., 2015](#)). Briefly, Sorted HSPCs were cross linked with 1% formaldehyde at room temperature for 10 min, and the reaction was stopped by 0.125M glycine at RT 5 min. Cross

linked cells were washed once with ice cold PBS containing protease inhibitor cocktail (GenDepot #P3100-001) and the cell pellet was stored at -80°C . Cells were thawed on ice and lysed in 50 μL lysis buffer (10 mM Tris pH 7.5, 1mM EDTA, 1% SDS), then diluted with 150 μL of PBS/PIC, and sonicated using Bioruptor (Diagenode) 30sec on 30 s off 7 cycles to 200-500 bp fragments. The sonicated chromatin was centrifuged at 4°C for 5 min at 13,000rpm to remove precipitated SDS. 180 μl was then transferred to a new 0.5 mL collection tube, and 180 μL of 2X RIPA buffer (20 mM Tris pH 7.5, 2 mM EDTA, 2%Triton X-100, 0.2% SDS, 0.2% sodium deoxycholate, 200 mM NaCl/PIC) was added to recovered supernatants. A 1 /10 volume (36 μl) was removed for input control. ChIP-qualified CTCF (Cell signaling #2899), H3K27ac (abcam #ab4729) and H3K27me3 (Millipore #07-449) antibodies were added to the sonicated chromatin and incubated at 4°C overnight. Previously washed 10 μL of protein A magnetic beads (Invitrogen #88846) were added and incubated for additional 2 hours at 4°C . Immunoprecipitated complexes were washed three times with RIPA buffer and twice with TE (10 mM Tris pH 8.0/1 mM EDTA) buffer. Following transfer into new 1.5 mL collection tube, genomic DNA was eluted for 2 hours at 68°C in 100 μl Complete Elution Buffer (20 mM Tris pH 7.5, 5 mM EDTA, 50 mM NaCl, 1% SDS, 50 $\mu\text{g}/\text{ml}$ proteinase K), and combined with a second elution of 100 μl Elution Buffer (20 mM Tris pH 7.5, 5 mM EDTA, 50 mM NaCl) for 10 min at 68°C . ChIPed DNA was purified by MinElute Purification Kit (QIAGEN #28006) and eluted in 12 μl elution buffer. ChIP-seq libraries were prepared using ThruPLEX-DNA library preparation kit without extra amplification (Rubicon #R400406). Paired-end 85bp sequencing was performed on Illumina NextSeq 500. The sequenced reads were aligned to the human genome (hg19) using Bowtie2 (version 2.2.1) allowing at most two mismatches. H3K27ac and CTCF enriched regions were determined using Model-based Analysis of ChIP-Seq (MACS) 2.1.1 using a p value threshold of 1e-9. For H3K27me3, the -broadPeaks flag was used to call enriched regions. Tracks were generated using bedtools genomecov (version 2.25.0) to compute coverage across the entire genome.

CTCF occupancy and orientation

The list of loops called by HiCCUPS was split into 4 groups based on the length of the loops: 0-1Mb, 1-2Mb, 2-3Mb and over 3Mb. Then the loops within each group were split into anchors and overlapping anchors were merged using bedtools. Anchors smaller than 15kb were expanded to 15kb and the number of anchors that overlap with at least one CTCF ChIP-seq peaks were counted using bedtools. We calculated fold enrichment of CTCF occupancy by comparing the counts with the average overlap of ten random translational controls with the same length distribution as the loop anchors. Orientation of CTCF motifs at loop anchors was identified using MotifFinder in Juicer ([Durand et al., 2016b](#)). Only loop anchors with a unique CTCF motif identified were included in the calculation. Similarly, we took the list of long loops annotated by hand, split the long loops into anchors, merged overlapping anchors, and counted the number of anchors that overlap with at least one CTCF ChIP-seq peak. Orientation of CTCF motifs at long loop anchors was identified using MotifFinder in Juicer. Only long loop anchors with a unique CTCF motif identified were included in the calculation.

RNA-Seq

Total RNA was extracted from cells using RNeasy mini kit (QIAGEN). RNA-seq was performed using the illumine Truseq Stranded mRNA library kit (Illumina #RS-122-2101). Total RNA was isolated from the sorted HSCs using RNeasy micro kit (QIAGEN #28006) together with RNase-free DNase treatment on the column (QIAGEN #79254). RNA samples were poly-A selected and fragmented at 94 for 8 min. First strand and second strand cDNA synthesized and followed by A-tailing and adaptor ligation. Ligated double strand libraries are purified and amplified 8-9 cycles. Multiplexed libraries are pooled and paired-end 85bp sequencing was performed on Illumina NextSeq 500. Reads were mapped to the genome using hisat2 (version 2.0.4). Transcript assembly was performed using cuffquant followed by cuffnorm mapped to hg19 refSeq annotation.

Aggregated peak analysis (APA) of canyon interaction

The original APA was implemented in Juicer ([Durand et al., 2016b](#)). To accommodate inter-chromosomal interaction probing and varying color scales, we implemented a revised version of APA for canyon interactions. To check for interaction patterns across distances, we implemented APAvsDistance, which completes Aggregate Peak Analysis (APA) on multiple sets of peaks in a contact matrix, where each set is defined by a range of distances, containing peaks with anchors separated by a distance within that pre-determined range. We divided a list of canyons into subgroups based on length or histone activity. For each subgroup, we paired the canyons using an all-by-all method, generating a list of 2D locations where canyons could interact in theory. The locations are binned based on the distance between the anchoring canyons, with each bin covering a predetermined range. APA was run on the list of locations in each bin at 10Kb resolution. The resulting APA plot and APA score show the aggregate signal from the listed locations in each bin, and collectively show the change in aggregate signal when anchoring canyons are separated at different distances in the respective subgroup. In addition, we generated lists of inter-chromosomal interactions for canyons in each subgroup and ran APA on those lists. As control, we ran APAvsDistance on HiCCUPS loops in HSPC and three published *in situ* Hi-C datasets: GM12878, IMR90 and HMEC. The loop lists were split into anchors and using an all-by-all method, generating a list of 2D locations where loop anchors could interact in theory. The original loop list is excluded to remove bias as those locations definitely carry strong peak signal.

APA analysis on published Hi-C data

APA from Juicer was run using lists of HSPC loops, HSPC loops with convergent CTCF, HSPC loops with HSPC repressive grand canyons, HSPC Long loops without HSPC repressive grand canyons, HSPC Long loops with HSPC repressive grand canyons, pairs

of HSPC repressive grand canyons and pairs of mouse HSC repressive grand canyons on published *in situ* Hi-C datasets at 10Kb resolution. The peak enrichment in HSPC was set to 100% and the peak enrichment in the other maps were calculated as a percentage of the peak enrichment in HSPC.

Cross sample H3K27me3 ChIP-seq analysis and data visualization

H3K27me3 and corresponding ChIP-seq reads were trimmed to exclude low quality bases and adaptor sequences using Trim Galore (v0.5.0). The trimmed reads were then mapped to the hg19 reference genome with bowtie2(v2.4.3)([Langmead and Salzberg, 2012](#)). uniquely alignments were kept for downstream analysis. For visualization of H3K27me3 signal over grand canyons, canyons, cUMRs and their flanking 5kb regions, bamCompare(deeptools v3.1.3) was used to count RPKM(duplicates were ignored, with signal of input subtracted) of each 100bp bin([Ramírez et al., 2014](#)).